3-15-2010

Vesicular Calcium Regulates Coat Retention, Fusogenicity, and Size of Pre-Golgi Intermediates

Marvin Bentley

Deborah C. Nycz

Ashwini Joglekar

Ismene Fertschai

Roland Malli

See next page for additional authors

Molecular Biology of the Cell
Vol. 21, 1033–1046, March 15, 2010

Vesicular Calcium Regulates Coat Retention, Fusogenicity, and Size of Pre-Golgi Intermediates

Marvin Bentley,*† Deborah C. Nycz,*† Ashwini Joglekar,‡§ Ismene Fertschai,‖ Roland Malli,‖ Wolfgang F. Graier,‖ and Jesse C. Hay*

*Division of Biological Sciences and Center for Structural and Functional Neuroscience, The University of Montana, Missoula, MT 59812-4824; ‡Department of Molecular, Cellular, and Developmental Biology, University of Michigan, Ann Arbor, MI 48109; and ‖Center of Molecular Medicine, Medical University of Graz, 8010 Graz, Austria

Submitted November 2, 2009; Revised December 17, 2009; Accepted January 13, 2010
Monitoring Editor: Adam Linstedt

The significance and extent of Ca^{2+} regulation of the biosynthetic secretory pathway have been difficult to establish, and our knowledge of regulatory relationships integrating Ca^{2+} with vesicle coats and function is rudimentary. Here, we investigated potential roles and mechanisms of luminal Ca^{2+} in the early secretory pathway. Specific depletion of luminal Ca^{2+} in living normal rat kidney cells using cyclopiazonic acid (CPA) resulted in the extreme expansion of vesicular tubular cluster (VTC) elements. Consistent with this, a suppressive role for vesicle-associated Ca^{2+} in COPII vesicle homotypic fusion was demonstrated in vitro using Ca^{2+} chelators. The EF-hand–containing protein apoptosis-linked gene 2 (ALG-2), previously implicated in the stabilization of sec31 at endoplasmic reticulum exit sites, inhibited COPII vesicle fusion in a Ca^{2+}-requiring manner, suggesting that ALG-2 may be a sensor for the effects of vesicular Ca^{2+} on homotypic fusion. Immunoisolation established that Ca^{2+} chelation inhibits and ALG-2 specifically favors residual retention of the COPII outer shell protein sec31 on pre-Golgi fusion intermediates. We conclude that vesicle-associated Ca^{2+}, acting through ALG-2, favors the retention of residual coat molecules that seem to suppress membrane fusion. We propose that in cells, these Ca^{2+}-dependent mechanisms temporally regulate COPII vesicle interactions, VTC biogenesis, cargo sorting, and VTC maturation.

INTRODUCTION

Although Ca^{2+} is a required cofactor in many types of exocytosis, it has been less clear what role Ca^{2+} plays in the constitutive membrane fusion reactions constituting the secretory and endocytic pathways. Indications that Ca^{2+} is required for constitutive trafficking have come from studies of endoplasmic reticulum (ER)-to-Golgi trafficking (Beckers and Balch, 1989), intra-Golgi transport (Porat and Elazar, 2000), endosome and lysosome fusion (Colombo *et al*., 1997; Peters and Mayer, 1998; Pryor *et al*., 2000). In most cases, fusion is inhibited by the fast Ca^{2+} chelator 1,2-bis(2-aminophenoxy)ethane-*N*,*N*,*N*′,*N*′-tetraacetic acid (BAPTA), but not by EGTA, a slower chelator of comparable affinity. This has led to the conclusion that Ca^{2+} must play its required role during a short pulse (<1 ms) of released luminal Ca^{2+} or else a Ca^{2+} gradient localized very near the transport machinery (Chen *et al*., 2002; Burgoyne and Clague, 2003; Hay, 2007). It has also been suggested that constant leakage of luminal Ca^{2+} from the ER and/or Golgi may create perpetual Ca^{2+} gradients surrounding these organelles; steady-state Ca^{2+} gradients around secretory organelles have been suggested by Ca^{2+} imaging techniques (Wahl *et al*., 1992). Basal Ca^{2+} leak from secretory organelles displays properties indicative of an ion-conducting channel; however, the most significant proteins responsible remain debatable (Camello *et al*., 2002). However important luminal Ca^{2+} may be at some stages of trafficking, luminal Ca^{2+} does not seem to play a universal role as a trigger of membrane fusion, because membrane-permeant chelators added to intact cells revealed a mosaic of Ca^{2+}-dependent and Ca^{2+}-independent transport steps (Chen *et al*., 2002). Little progress has been made in elucidating mechanisms of Ca^{2+} action in constitutive trafficking, although there are a few interesting hints. Calmodulin antagonists have implicated this effector in several constitutive transport steps that require Ca^{2+} (Burgoyne and Clague, 2003); downstream targets may include Ca^{2+}-dependent protein kinase II, soluble *N*-ethylmaleimide-sensitive factor attachment protein receptors (SNAREs), and vesicle tethers (Colombo *et al*., 1997; Mills *et al*., 2001; De Haro *et al*., 2003). Other Ca^{2+} effectors in the constitutive secretory pathway include the coat proteins responsible for transport vesicle formation. Membrane-permeant BAPTA destabilizes COPI binding to membranes in vivo (Ahluwalia *et al*., 2001). Furthermore, the penta-EF-hand (PEF) protein apoptosis-linked gene (ALG)-2 is present at ER exit sites, and, when Ca^{2+} is present, stabilizes association of

This article was published online ahead of print in *MBC in Press* (http://www.molbiolcell.org/cgi/doi/10.1091/mbc.E09–10–0914) on January 20, 2010.

† These authors contributed equally to this work.

§ Present address: Evolvus, Inc., Pune, India.

Address correspondence to: Jesse C. Hay (jesse.hay@umontana.edu).

Abbreviations used: ALG, apoptosis linked gene; CPA, cyclopiozonic acid; ERES, endoplasmic reticulum exit site; ERGIC, endoplasmic reticulum-Golgi intermediate compartment; NRK, normal rat kidney; SNARE, soluble *N*-ethylmaleimide-sensitive factor attachment protein receptor; VSV-G*, radiolabeled vesicular stomatitis virus glycoprotein ts045; VSV-G-myc, myc-tagged vesicular stomatitis virus glycoprotein ts045; VTC, vesicular tubular cluster.

the sec31 COPII subunit at the membrane (Yamasaki *et al.*, 2006; la Cour *et al.*, 2007; Shibata *et al.*, 2007).

Vesicle coats such as COPII, COPI, and assembly protein (AP)-clathrin concentrate cargo and deform membranes to form spherical vesicles with highly sorted membrane and luminal contents (Barlowe *et al.*, 1994). The traditional view has held that shortly after vesicle budding, guanosine triphosphate (GTP) hydrolysis by sar or arf would trigger coat depolymerization and its quantitative loss from the membrane (Bonifacino and Glick, 2004). This view was reinforced by the presence of GTPase activation protein (GAP) activities intrinsic to coats, naturally leading to the idea of concerted coat dissolution after budding. Recently, however, evidence has accumulated that at least a portion of some coats remains on vesicles during the docking phase and in fact assists this function by serving as targeting sites for tethers. This represents a new information-encoding function for coats in vesicle transport. For example, the COPII inner shell subunit sec23 serves as a targeting site for the tether mBet3 of transport protein particle (TRAPP)I and is required for successful homotypic COPII vesicle tethering in mammals and COPII vesicle-Golgi tethering in yeast (Cai *et al.*, 2007). Immunoisolation of mammalian pre-Golgi intermediates after tethering reactions revealed stably associated pools of inner and outer shell COPII components, although the exact stage after TRAPP-mediated tethering at which the residual coat is shed has not been determined (Cai *et al.*, 2007).

Much of the machinery for ER-to-Golgi transport has been identified. In mammalian cells, cargo moves from the ER to Golgi in pleomorphic vesicular tubular clusters (VTCs) that travel along microtubules (Presley *et al.*, 1997; Scales *et al.*, 1997). VTCs are part of a broader network of vesicles and tubules often referred to as the ER-Golgi intermediate compartment (ERGIC) (Saraste and Svensson, 1991). Some VTCs may be long lived and relatively immobile sorting stations that give rise to the transient, mobile structures (Ben-Tekaya *et al.*, 2005). ER-to-Golgi cargo transport must involve at least two membrane fusions—one fusion to transfer cargo from COPII vesicles into VTCs in the periphery of the cell—and a second fusion to transfer cargo from Golgi-centric VTCs into the *cis*-Golgi (or alternatively to create the *cis*-Golgi de novo). COPII vesicles in vitro contain all components necessary for homotypic tethering and fusion to form nascent VTCs (Xu and Hay, 2004; Bentley *et al.*, 2006). Thus, homotypic COPII vesicle fusion seems to represent at least one pre-Golgi membrane fusion contributing to VTC biogenesis and anterograde transport. Rab1 seems to represent a coordinating factor for ER-to-Golgi transport and has several effectors (Allan *et al.*, 2000). These include the golgins p115 (Uso1p in yeast) and GM130, which are required for ER-to-Golgi transport (Alvarez *et al.*, 2001; Moyer *et al.*, 2001); p115 is also required for in vitro homotypic COPII vesicle tethering and fusion (Bentley *et al.*, 2006). The seven-member TRAPP complex includes subunits mbet3 and sedlin, is required for ER-to-Golgi transport, and seems to represent a tethering factor for COPII vesicles and a guanine nucleotide exchange factor for rab1 (Sacher *et al.*, 2001; Loh *et al.*, 2005; Yu *et al.*, 2006). Both the golgin p115 and TRAPP have been implicated as tethering machinery for COPII vesicles; their precise functional relationship remains to be determined. The fusion machinery consists of SNARES syntaxin 5, membrin, rbet1, and sec22b, which form a well-characterized quaternary complex that has served as a prototype for intracellular SNARE complexes (Xu *et al.*, 2000; Joglekar *et al.*, 2003; Xu and Hay, 2004).

This study was designed to investigate the potential role and molecular mechanism of luminal Ca^{2+} in early steps in ER-to-Golgi transport. We found that luminal Ca^{2+} dramatically influences VTC size and distribution in cells. Furthermore, we examined the potential role of the EF-hand–containing protein ALG-2 and its coat-stabilizing activity as effectors of luminal Ca^{2+} to regulate COPII vesicle fusion and VTC biogenesis.

MATERIALS AND METHODS

Depletion of Luminal Calcium

Ca^{2+}-free DMEM (D9802-05B; US Biological, Swampscott, MA) was supplemented with 10% fetal bovine serum that had been dialyzed (twice for 2 h) in a 100-fold excess of Ca^{2+}-free phosphate-buffered saline (PBS). Cells to be depleted of luminal Ca^{2+} were washed twice with Ca^{2+}-free DMEM/10% fetal bovine serum (FBS) containing 10 μM cyclopiazonic acid (CPA; C1530, Sigma-Aldrich, St. Louis, MO), 1 mM EGTA, and 25 mM HEPES, pH 7.2, and then incubated in that medium for 15 min. This was followed by an incubation (usually 15 min) in Ca^{2+}-free DMEM/10% FBS, no CPA, 0.3 mM EGTA, and 25 mM HEPES, pH 7.2. Some treatments included 10 μg/ml cycloheximide for a 30-min period before addition of CPA; in these cases, cycloheximide was also maintained in the medium during the CPA treatment and subsequent Ca^{2+}-free chase. A 30-min cycloheximide pretreatment has been shown to block ATF6 activation by thapsigargin in HeLa and COS cells (Haze *et al.*, 1999).

Immunofluorescence

For immunofluorescence, coverslips were dropped directly into wells of room temperature 4% paraformaldehyde in 0.1 M sodium phosphate, pH 7.0, for 30 min. Samples were then quenched twice for 10 min with 0.1 M glycine in PBS. Cell permeabilization was then carried out for 15 min at room temperature by using permeabilization solution (0.4% saponin, 1% bovine serum albumin [BSA], and 2% normal goat serum in PBS), followed by incubation in primary antibodies diluted in permeabilization solution for 1 h at room temperature. After three rigorous washes with permeabilization solution, the coverslips were incubated with secondary antibodies diluted in the same buffer for 30 min, followed by three more washes. For immunofluorescence of Sec16, coverslips were washed with PBS and then fixed for 10 min at −20°C in 100% methanol, and the antibody incubation/wash solution was PBS, pH 7.5, plus 1% BSA. Coverslips were mounted using Vectashield anti-fade solution (Vector Laboratories, Burlingame, CA) and analyzed using an E800 microscope (Nikon, Tokyo, Japan) with a 60× plan APO numerical aperture 1.40 objective. Images were collected using an ORCA 2 digital camera (Hamamatsu, Bridgewater, NJ) controlled by OpenLab software (Improvision, Coventry, United Kingdom). Images for quantitation were collected in a consistent manner with regard to cell morphology, protein labeling intensities, and exposure. After choosing a fixed exposure time for each color channel that would accommodate the majority of cells, we avoided any cell whose intensity values in any color exceeded the saturation value of 16383 or fell below 4000 on our 14-bit acquisition system. We also avoided capturing cells lacking a flat morphology and single, well-defined nuclei surrounded on all sides by an expanse of cytoplasm. Only cells exhibiting relatively strong and clear rbet1 labeling were selected. An image stack was collected for each color channel for each field of cells randomly encountered containing at least one cell that met the necessary objective criteria for quantification.

Quantification of Images

Separate excitation and emission filter wheels equipped with fluorescein isothiocyanate (FITC) and cyanine (Cy)3 filter sets were used, and 21 image planes were captured in 0.2-μm increments. Images were deconvolved using Huygens Essential Widefield software (Scientific Volume Imaging, Hilversum, The Netherlands). For a given field, a single image plane containing rbet1 labeling in focus in the peripheral cytoplasm was selected, and the background labeling was removed by defining a dark extracellular area of the image as zero using the automation tool in OpenLab. An rbet1 object binary image mask was generated by thresholding rbet1 labeling at 4 times over its intensity in a peripheral area lacking punctate objects (i.e., the labeling of rbet1 in the ER). A Golgi mask was then created by thresholding the GM130 labeling at 25% of its maximum intensity. The Golgi mask was subtracted from the rbet1 object mask using Boolean operations to generate a peripheral rbet1 object mask; this mask was used to identify and quantify pixels within peripheral rbet1 objects. Peripheral p24 objects were quantified in the same manner using a Golgi mask.

Antibodies

Monoclonal anti-rbet1 antibodies were described previously (Hay *et al.*, 1998). Affinity-purified polyclonal anti-p24, -sec23, and -β-COP from our laboratory

were described previously (Bentley *et al*., 2006). Anti-sec31 was produced in rabbits against the synthetic peptide KLKEIDRTAMQAWSPAQNHPC and then affinity purified using a column of the immobilized peptide. Anti-GM130 and -p115 were a kind gift from Dr. Martin Lowe (University of Manchester, Manchester, United Kingdom). Anti-ALG-2 was a kind gift from Dr. Masayuki Komada (Tokyo Institute of Technology, Tokyo, Japan). Anti-sec16 antibody (KIAA0310) was acquired from Novus Biologicals (Littleton, CO). Anti-GPP130 antibody (PRB144C) was purchased from Covance Research Products (Princeton, NJ). Anti-protein disulfide isomerase (PDI; SPA-890) was from Assay Designs (Ann Arbor, MI). Anti-IP3R-3 (610312) was purchased from BD Biosciences Transduction Laboratories (Lexington, KY). Anti-mannosidase II antibody (MMS-110R-200) was purchased from Covance Research Products. Anti-myc monoclonal antibody (mAb) 9E10 was purified from hybridoma tissue culture supernatant. Secondary antibodies were FITC or Cy3 conjugated and purchased from Jackson ImmunoResearch Laboratories (West Grove, PA).

Luminal Ca^{2+} Measurements

Normal rat kidney (NRK) cells (~80% confluent) were transiently transfected with 1.5–2 μg of purified plasmid DNA of the respective Ca^{2+} sensor using TransFast (Promega, Vienna, Austria) as described previously (Trenker *et al*., 2007). Cells were used for experiments at ~48 h after transfection. YC3.6 (Nagai *et al*., 2004) and YC2.1 (Miyawaki *et al*., 1997) were used to monitor the free Ca^{2+} concentration in the cytosol, and D1ER (Palmer *et al*., 2004) was used to monitor free Ca^{2+} within the ER lumen (Malli *et al*., 2005; Osibow *et al*., 2006). The fluorescence resonance energy transfer-based Ca^{2+} sensor D1ER was excited at 440 ± 21 nm (440AF21; Omega Optical, Brattleboro, VT), and emission was collected simultaneously at 535 and 480 nm with a single camera using an optical beam splitter (535 and 480 nm, Dual-View MicroImager; Optical Insights, Visitron Systems, Puchheim, Germany). $[Ca^{2+}]$Cyto was calculated from the normalized ratio values $Ratio_{i^n} = \left(\frac{(F_i^{535}/F_i^{480})}{(F_0^{535}/F_0^{480})}\right)$ using the following equation: $[Ca^{2+}] = K_D \cdot \left(\frac{Ratio_{i^n} - Ratio_{\min}}{Ratio_{\max} - Ratio_{i^n}}\right)$ μM (Osibow *et al*., 2006). The K_D value for YC3.6 was assumed to be 250 nM (Nagai *et al*., 2004). For the calculation of $[Ca^{2+}]_{ER}$, the raw D1ER recordings ($Ratio\ F^{535}/F^{480}$) were corrected for bleaching using a calculated individual bleaching-function (R0) by subtracting R0 from the raw $Ratio\ F^{535}/F^{480}$. From this curve the respective $Ratio_i$, $Ratio_{min}$, and $Ratio_{max}$ values were extracted and $[Ca^{2+}]_{ER}$ was calculated using the equation above. The K_D value of D1ER in situ for calculating $[Ca^{2+}]_{ER}$ was assumed to be 220 μM according to Rudolf *et al*. (2006). $Ratio_{min}$ and $Ratio_{max}$ were determined using 1 μM ionomycin in 1 mM EGTA and subsequently in 2 mM Ca^{2+}-containing solution, respectively, for each single measurement (cytosolic Cameleons and D1ER). Statistical data for Ca^{2+} measurements are presented as mean ± SEM. Analysis of variance and Scheffé's post hoc F test were used for evaluation of the statistical significance, with $p < 0.05$ defined as significant.

Cloning, Expression, and Purification of Recombinant Proteins

A mouse ALG-2 cDNA clone (IMAGE:3156800; MGC:49479) was purchased from American Type Culture Collection (Manassas, VA). The full-length coding region was amplified using polymerase chain reaction (PCR) and specific primers to incorporate XbaI and XhoI restriction sites: 5′-CCATATTCTAGACGCTGCCTACTCCTACCGCCC-3′ (coding strand) and 5′-CCATATCTCGAGTTATACAATGCTGAAGACC-3′ (noncoding strand). The amplified ALG-2 fragment was subcloned into the XbaI/XhoI cloning sites of the pGEX-KG expression vector (Guan and Dixon, 1991) to construct the GST-ALG-2 expression vector. We used QuikChange PCR mutagenesis (Stratagene, La Jolla, CA) to introduce E47→A and E114→A mutations into the ALG-2 EF hands 1 and 3, respectively. Using the GST-ALG-2 construct as template, the following mutagenesis primers were used: E47A, 5′-GGAGTGATTCAGACAATGCGCTTCAGCAAGCATTATCC-3′ (coding strand) and 5′-GGATAATGCTTGCTGAAGCGCATTGTCTGAAATCACTCC-3′ (noncoding strand); and E114A, 5′-GGATGATTGACAAGAACGCGCTCAAACAAGCACTCTC-3′ (coding strand) and 5′-GAGAGTGCTTGTTTGAGCGCGTTCTTGTCAATCATCC-3′ (noncoding strand). All expression constructs were verified by sequencing of the entire insert. The resulting GST-ALG-2 wild-type and double mutant expression vectors were transformed into *Escherichia coli* NM522 for protein expression.

GST-ALG-2, GST-ALG-2 E47,114A, and glutathione transferase (GST) control strains were grown in Luria broth at 37°C to an A_{600} of 0.4–0.6 and induced with 0.1 mM isopropyl-1-thio-β-D-galactopyranoside (IPTG) for 2–3 h. After harvesting the cultures, each 3-l culture of bacteria was resuspended in 60 ml of French Press buffer (50 mM Tris, pH 8.0, 0.1 M NaCl, 1 mM EDTA, 1 mM dithiothreitol [DTT], and protease inhibitors [Complete EDTA-free; Roche Applied Science, Indianapolis, IN)], disrupted twice with a French Press and clarified by centrifugation at 20,000 × *g* for 20 min followed by 100,000 × *g* for 1 h. The final supernatants were applied to a 2-ml glutathione-Sepharose column (GE Healthcare, Little Chalfont, Buckinghamshire, United Kingdom), equilibrated, and washed extensively with PBS, and then eluted with 50 mM Tris, pH 8.0, 20 mM glutathione. The eluted protein was then dialyzed extensively in 25/125 buffer (25 mM HEPES, pH 7.2, and 125 mM potassium acetate) and stored in single-experiment aliquots at −80°C.

GST-sar1a T39N in a pGEX vector was obtained from Drs. Jinoh Kim and Randy Schekman (University of California–Berkeley, Berkeley, CA). Three liters of culture was grown in Luria broth containing 100 μg/ml ampicillin at 37°C to an optical density of 0.4–0.6, and then protein expression was induced by addition of 0.1 mM IPTG for 2 h. Bacterial pellets were resuspended in French Press buffer containing 1 mM DTT, 10 μM guanosine diphosphate (GDP), and 5 mM magnesium acetate, and a soluble extract was prepared as for GST-ALG-2 described above. The final extract was loaded onto a 2-ml glutathione-Sepharose column, washed with PBS containing 10 μM GDP and 5 mM magnesium acetate, and eluted with 50 mM Tris, pH 8.0, 20 mM glutathione, 10 μM GDP, and 5 mM magnesium acetate. The purified GST-sar1a T39N was then digested with thrombin, dialyzed extensively against 25/125 buffer containing 10 μM GDP and 5 mM magnesium acetate, and stored at −80°C.

Heterotrimerization Fusion Assays

COPII vesicle fusion experiments (see Figures 3, 5, and 6) were carried out as described previously (Xu and Hay, 2004; Bentley *et al*., 2006; Cai *et al*., 2007). In brief, the vesicular stomatitis virus-glycoprotein (VSV-G)-myc–expressing NRK cells and pulse-radiolabeled VSV-G*–containing cells were permeabilized by scraping with a rubber policeman and then washed and resuspended at ~170 μl/10-cm plate in 50/90 buffer (50 mM HEPES, pH 7.2, and 90 mM potassium acetate). A first-stage (vesicle release) incubation to produce enough vesicles for a 24-point fusion assay contained 1.96 ml and consisted of 432 μl of water, 67.5 μl of 0.1 M magnesium acetate, 135 μl of ATP-regenerating system, 40.5 μl of 1 M HEPES, pH 7.2, 270 μl of weak calcium buffer (20 mM HEPES, pH 7.2, 1.8 mM $CaCl_2$, and 5 mM EGTA), 675 μl of dialyzed rat liver cytosol, and 337.5 μl of either of the permeabilized cell populations. After incubation at 32°C for 30 min to allow vesicle release, cells were removed by centrifugation at 4000 × *g* for 1 min followed by 15,000 × *g* for 1 min. The supernatant, which contains released COPII vesicles, was saved. For the second-stage fusion incubations, each reaction totaled 200 μl and contained 72.5 μl of VSV-G-myc vesicles, 72.5 μl of VSV-G* vesicles, and 55 μl of 25/125 buffer or test components dissolved in 25/125 buffer. It was at this point that proteins such as GST-ALG-2 or test chelators such as BAPTA were added. After a 20-min preincubation on ice with these test components, the reactions were incubated at 32°C for 60 min to allow tethering, fusion, and heterotrimerization between VSV-G-myc and VSV-G* vesicles. For measuring heterotrimers, the final vesicle suspensions were supplemented with 2% Triton X-100, incubated with agitation at 4°C for 20 min, and then centrifuged at 100,000 × *g* for 30 min. The 100,000 × *g* supernatants containing solubilized VSV-G trimers were then processed for immunoprecipitation by using 5 μg of biotinylated anti-myc antibodies and 5 μl (packed) streptavidin-Sepharose (GE Healthcare). Immunoprecipitates were solubilized in SDS sample buffer, analyzed by SDS-polyacrylamide gel electrophoresis (PAGE; 8%) and phosphorimaging, and coprecipitated VSV-G* was quantified.

For immunoblotting of transport intermediates such as in Figure 4, a similar setup to that described above was used except that only VSV-G-myc–expressing cells were used because radioactivity was inconsequential to this assay. After scraping and washing as described above, the cells were resuspended in ~170 μl of 50/90 buffer/10-cm plate. Each immunoisolation condition involved a reaction volume of 600 μl and contained 96 μl of water, 15 μl of 0.1 M magnesium acetate, 30 μl of ATP-regenerating system, 9 μl of 1 M HEPES, pH 7.2, 60 μl of weak calcium buffer (see above), 150 μl of dialyzed rat liver cytosol, 165 μl of 25/125 buffer or test proteins dialyzed in this buffer, and 75 μl of VSV-G-myc–expressing or control NRK cells. In certain control reactions, 800 nM sar1 T39N or 100 μM guanylylimidodiphosphate (GMP-PNP) were included to block COPII budding or uncoating, respectively. After incubation at 32°C for 30 min to allow vesicle release, cells were removed by centrifugation at 4000 × *g* for 1 min followed by 15,000 × *g* for 1 min. The supernatant, which contains released COPII vesicles, was then supplemented with test proteins such as GST-ALG2 or chelators and incubated another 1 h at 32°C to allow tethering and fusion. The suspension of tethered/fused vesicles was then subjected to immunoisolation. This was accomplished by addition 5 μg of anti-myc antibody and incubation for 2 h at 4°C with end-over-end rotation at 3 rpm. The suspension was then supplemented with 15 μl (packed) of protein A-Sepharose beads (preblocked in 5 mg/ml BSA and 5 mg/ml PVP-40T in 25/125 buffer) and incubated at 4°C overnight with slow end-over-end rotation. Beads were washed four times by centrifugation at 375 × *g* for 1 min and resuspension in 25/125 buffer containing 1 mg/ml BSA. During the last wash, resuspended beads were transferred to a fresh tube. After the washes, proteins were eluted from the beads by addition of 50 μl of 0.1 M glycine, pH 2.5, mixing, centrifugation at 375 × *g* for 1 min, and removing the supernatant to a tube containing 7.5 μl of 2 M Tris, pH 8.0. Elution was repeated twice more into this eluate pool (157.5 μl of total eluate), and the eluate pool was placed into a Microcon YM-10 ultrafiltration device (Millipore, Billerica, MA) and centrifuged to dryness. The sample on the membrane was dissolved in 25 μl of SDS sample buffer and analyzed by 4–20% gradient SDS-PAGE gels and immunoblotting.

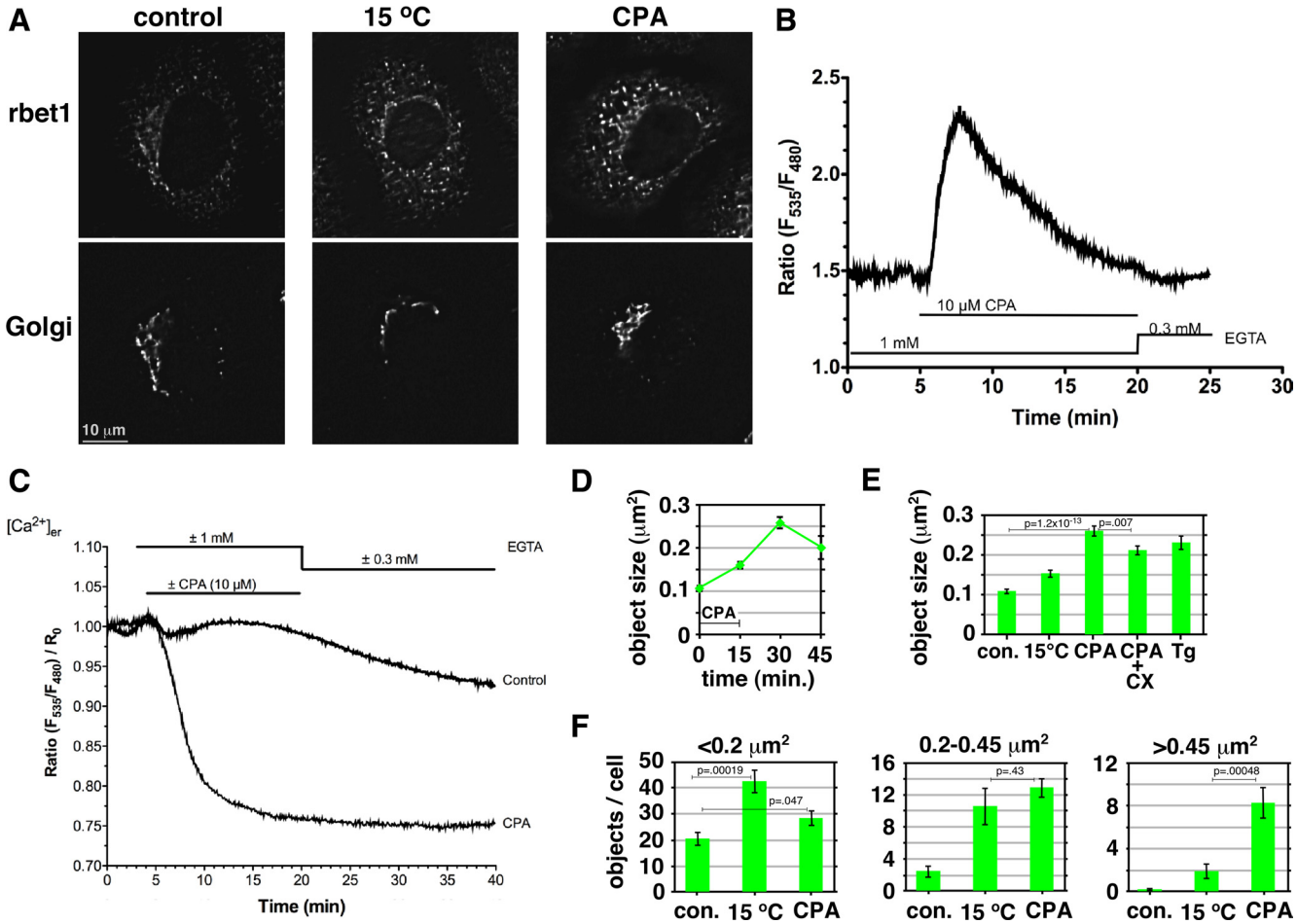

Figure 1. Luminal Ca^{2+} regulates size of rbet1-positive pre-Golgi structures. (A) NRK cells were either mock treated, incubated at 15°C for 30 min, or treated with CPA to deplete luminal Ca^{2+} (see *Materials and Methods*), and then fixed and immunostained for rbet1 and the Golgi marker GM130. Shown are single focal planes from deconvolved widefield image stacks. (B) Cytosolic Ca^{2+} dynamics during the CPA regimen to deplete luminal Ca^{2+}. Fluorescence ratios are calibrated to free Ca^{2+} values in Supplemental Figure S1A. (C) Luminal ER Ca^{2+} dynamics during the CPA regimen. Fluorescence ratios are calibrated to free Ca^{2+} values in Supplemental Figure S1B. (D–F) Quantitation of peripheral rbet1-positive objects in experiments such as described in A. Values represent per cell means derived from at least 20 randomly chosen cells. Error bars display SE. CX, cycloheximide; Tg, thapsigargin. In F, only objects that fall within the size bins indicated above each plot are included in each panel. Selected p values from two-tailed Student's *t* test are included. Areas of objects were calculated assuming that one image pixel width calibrates to 224 nm in the cell. Single-pixel objects (with calculated area 0.05 μm^2) are subresolution but were not eliminated from the size analysis; they did not contribute to the 0.2–0.45 μm^2 and >0.45 μm^2 size bins in F.

Chelator Studies

Under our basal in vitro assay conditions described above, in the absence of "test" chelators, our fusion reactions were weakly Ca^{2+} buffered to approximately resting cytosolic free Ca^{2+} conditions. In the presence of 500 μM EGTA, 2.5 mM total Mg^{2+}, 180 μM total $CaCl_2$, at pH 7.2, calculations suggest 63 nM free Ca^{2+}(Portzehl *et al.*, 1964). This minimal buffering system was necessary to offset variations in Ca^{2+} that might be present in different batches of cytosol and other reagents used in experiments but was easily superseded by adding millimolar concentrations of chelators that are typically necessary to neutralize biological Ca^{2+} transients. For example, addition of an extra 5 mM EGTA, as in Figure 3A, is calculated to reduce equilibrium free Ca^{2+} >10-fold to 3.6 nM.

RESULTS

Luminal Ca^{2+} Regulates Membrane Trafficking in the Early Secretory Pathway

Past studies on the role of Ca^{2+} in the biosynthetic secretory pathway have relied on membrane-permeant chelators that chelate cytosolic as well as luminal Ca^{2+} (Chen *et al.*, 2002) and thus do not elucidate a specific role for luminal Ca^{2+} per se. To begin to examine the role of luminal calcium in ER-to-Golgi trafficking, we used CPA, a reversible inhibitor of the sarco/endoplasmic reticulum Ca^{2+}-ATPase (SERCA) (Mason *et al.*, 1991). NRK cells were treated with CPA, and the distribution of the ER-to-Golgi SNARE rbet1, a type II integral membrane protein, was examined at various time points. If subtle changes in membrane flux between the ER and Golgi occurred, rbet1 distribution should be a sensitive indicator, because rbet1 rapidly cycles between the ER and Golgi and is largely localized to the ERGIC at steady state (Hay *et al.*, 1998). As shown in Figure 1A, CPA treatment in Ca^{2+}-free medium for 15 min followed by a 15-min chase period in Ca^{2+}-free medium resulted in a change in the appearance of rbet1. Control cells exhibit strong rbet1 labeling in the perinuclear area surrounding the Golgi marked by GM130 and fainter punctate structures in the peripheral cytoplasm that are not associated with Golgi. CPA-treated cells, in contrast, displayed relatively more intense punctate peripheral rbet1-positive objects compared with the perinu-

clear labeling. This change did not result from a dispersal of Golgi into the peripheral cytoplasm, as indicated by the GM130 labeling. As also shown in Figure 1A, the overall effect of CPA seemed similar to that when the cells were incubated at 15°C, a treatment that is commonly used to trap anterograde cargo and vesicle machinery in swollen, peripheral ERGIC structures (Saraste and Svensson, 1991).

To confirm that our protocol achieved specific depletion of luminal Ca^{2+} as intended, we used live imaging of luminal (Figure 1C and Supplemental S1B) and cytosolic (Figure 1B and Supplemental S1A) Ca^{2+}. Ca^{2+} concentrations were determined using transfected chameleon biosensors D1ER (Palmer *et al*., 2004) and YC3.6 (Nagai *et al*., 2004) that have optimal affinities for the free Ca^{2+} concentrations in the respective compartments. Treatment with 10 μM CPA resulted in a severe depletion of ER luminal free Ca^{2+} within 10 min of addition, from 385 μM, a typical resting value for cultured mammalian cells (Osibow *et al*., 2006; Malli *et al*., 2008), to 23 μM; this means that vesicular COPII-derived membranes generated from the ER after 10 min must also be depleted of vesicular Ca^{2+}. As expected, cytosolic Ca^{2+} underwent an extreme increase as the luminal compartment was emptied, but this was cleared and restored to the resting value of 45–50 nM after 15 min of CPA addition. We conclude that by the end of the 15-min CPA treatment and start of the chase period, luminal Ca^{2+} is depleted by >90% and cytosolic Ca^{2+} is at resting levels. Furthermore, this condition seems to remain stable during the chase period after CPA washout.

The increased peripheral rbet1 staining during CPA treatment can be observed quantitatively by measuring the average area of peripheral rbet1-positive objects over time (Figure 1D). The area of an average peripheral rbet1-positive structure more than doubled during the standard treatment condition of 15-min CPA plus 15 min Ca^{2+}-free chase. Most of the increase occurred during the chase period during which the desired condition of specific luminal depletion was achieved. Chase for an additional 15 min (30-min total) led to a slight decrease in object size; however, we believe this apparent decrease was an artifact of a gross morphology change in the cells, which began to round up during this interval. We compared the effect of CPA treatment on peripheral object size to other treatment conditions (Figure 1E). Luminal Ca^{2+} depletion by CPA treatment for 15 min and chase for 15 min caused a significantly more dramatic increase in object size than 15°C treatment for 30 min. CPA plus cycloheximide gave similar results to CPA, but less dramatic, demonstrating that the growth of rbet1 peripheral objects involves mostly redistribution of existing rbet1 rather than recruitment of newly synthesized protein. Cycloheximide also blocks the accumulation of unfolded proteins during ER luminal Ca^{2+} depletion and Ire1p-dependent transcriptional activation of ER stress response elements (Haze *et al*., 1999; Rüegsegger *et al*., 2001); thus, ER stress responses related to the accumulation of unfolded proteins seem unlikely to be an important determinant of the rapid changes in ERGIC structure observed with CPA. Thapsigargin, a distinct SERCA inhibitor (Mason *et al*., 1991), caused a similar effect on mean object size, confirming the mechanism of the CPA effect.

To observe subtle changes in size distribution, peripheral rbet1 objects were binned according to size (Figure 1F). Although the number of small objects (<0.2 μm^2) remained virtually unchanged in CPA-treated cells, CPA treatment clearly generates a new population of objects >0.45 μm^2. Interestingly, the 15°C treatment resulted in a different distribution of object sizes than the luminal Ca^{2+} depletion. Although 15°C caused an overall increase in the number of objects, most of the increase occurred in the <0.2-μm^{2+} size range, rather than in the large size bin as for CPA. We also noticed that the preferential creation of large objects by CPA treatment occurred at earlier time points (data not shown), indicating that increased numbers of small objects is not a kinetic intermediate on-pathway to the CPA effect of increased large objects. This suggests that the trafficking step(s) affected by the two treatments is distinct. For example, the CPA effect would be consistent with overactive fusion of COPII vesicles and VTCs and/or a lack of recycling from them, whereas the 15°C phenotype would be more consistent with a buildup of vesicles/VTCs due to a lack of microtubule-dependent transport.

Total rbet1 labeling intensity increased significantly in the CPA and 15°C treated cells (Supplemental Figure S2A). This could indicate either that more rbet1 was present after these treatments or that the pool of rbet1 in the trapped intermediates was more accessible for immunofluorescence labeling. This increase was specific to the rbet1 mAb used; in the same cells, total GM130 labeling intensity did not change (Supplemental Figure S2B). In addition, another protein that cycles rapidly through VTCs, p24, did not increase significantly in total intensity (Supplemental Figure S2D). Furthermore, rbet1 in the cell population did not change significantly as assessed by quantitative Western blotting (Supplemental Figure S2C). We conclude that the 16G6 N-terminal rbet1 epitope is more accessible in the swollen structures, perhaps indicating a change in SNARE protein interactions.

To test whether the luminal Ca^{2+} effect was specific to the rbet1 protein per se, the distribution of the rapidly recycling vesicle marker p24 was examined. As shown qualitatively in Figure 2A, p24 also increased in Golgi-negative, punctate peripheral objects upon luminal Ca^{2+} depletion. This change was similarly reflected quantitatively by a dramatic increase in the number of p24 objects >0.45 μm^{2+} (Figure 2C). However, unlike for rbet1, there was not a significant increase in p24 total integrated staining intensity (Supplemental Figure S2D). In conclusion, multiple ERGIC markers, and not just ER/Golgi SNAREs, rapidly accumulate in large peripheral structures upon luminal Ca^{2+} depletion.

The enlarged objects represent pre-Golgi intermediates because they are negative for Golgi markers; other possibilities include ER exit sites (ERESs) or vesicular tubular clusters (VTCs). We examined sec16, an ERES scaffold protein that is not part of the COPII vesicle coat per se (Hughes *et al*., 2009). As shown qualitatively in Figure 2B and quantitatively in Figure 2D, the number of above-threshold sec16-positive objects did not change significantly upon CPA treatment, in contrast to rbet1 objects quantified in the exact same cells. Hence, the enhanced peripheral structures do not seem to be caused by a general expansion or proliferation of ERES. Our results are consistent with a previous study using membrane-permeant chelators concluding that Ca^{2+} was involved at a post-ER but pre-Golgi step in VSV-G-green fluorescent protein (GFP) transport (Chen *et al*., 2002). If the expanded objects represent early-stage VTCs, one would expect them to be closely associated with both ERES as well as COPI components, due to the immediate proximity of nascent VTCs to ERES and their capacity to recruit COPI shortly after formation (Aridor *et al*., 1995; Rowe *et al*., 1996). For each cell in the populations quantified in Figure 2B after CPA treatment, the largest rbet1 peripheral structures, i.e., those most likely to represent a specific result of Ca^{2+} depletion, were analyzed in greater detail. In 98% of cases, these rbet1 objects overlapped by at least 50% of their area with a sec16 object. A similar experiment was carried out

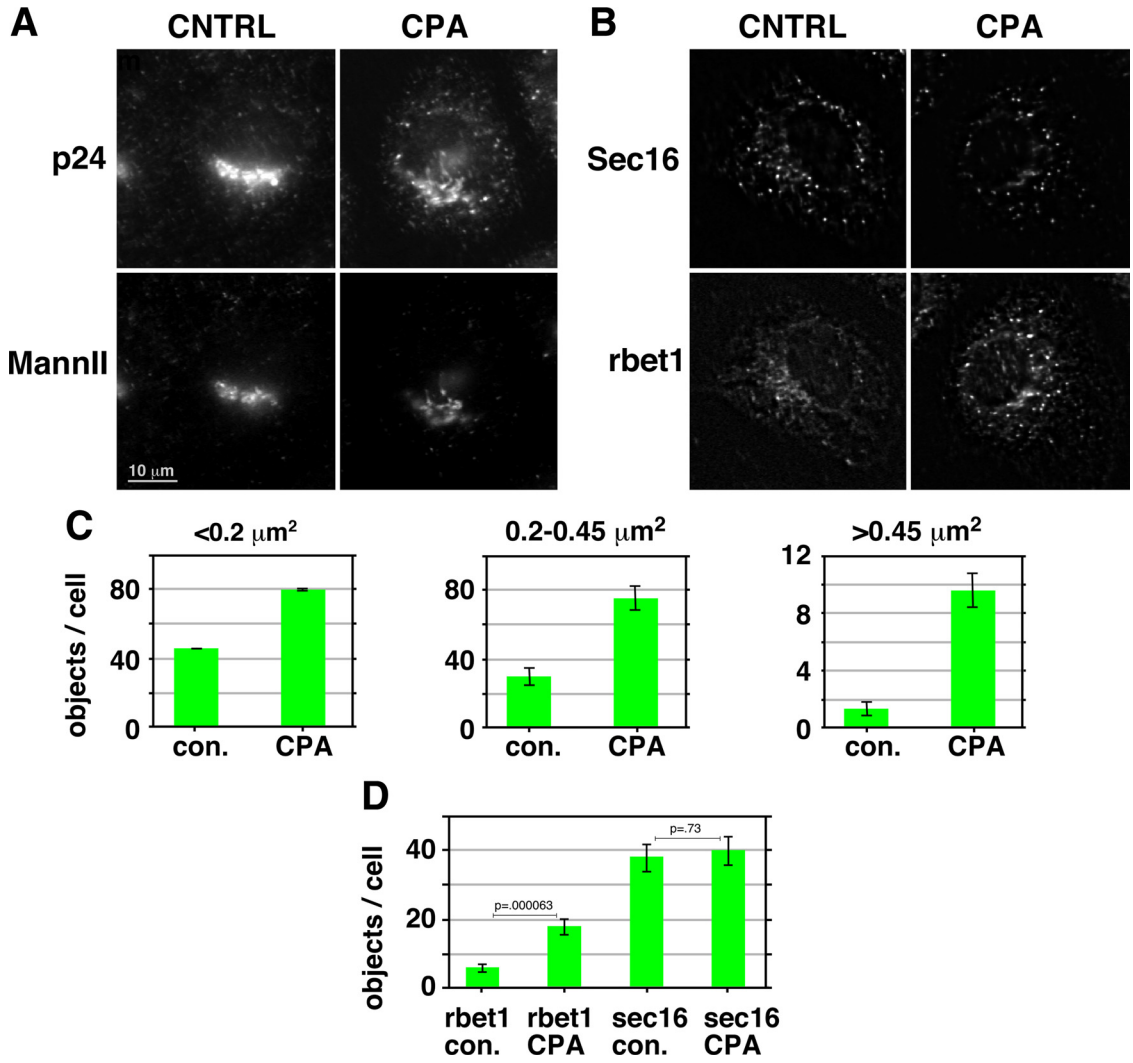

Figure 2. Luminal Ca^{2+} regulates the size of ERGIC but not ERES structures. (A) NRK cells were either mock treated or treated with CPA to deplete luminal Ca^{2+} (see *Materials and Methods*), then fixed and immunostained for p24 and the Golgi marker mannosidase II. Shown are single focal planes from deconvolved widefield image stacks. (B) Immunolabeling for rbet1 and sec16 under the same experimental conditions as described in A. (C) Quantitation of numbers of peripheral p24-positive objects in three size bins under the experimental conditions shown in A. (D) Quantitation of peripheral objects positive for rbet1 and sec16 from the experiment shown in B. All size bins were included in one analysis. The rbet1 and sec16 object data are from precisely the same set of double-labeled cells. Values represent means derived from at least 20 randomly chosen cells. Error bars display SE. Selected p values from two-tailed Student's *t* test are included.

using rbet1/β-COP costaining and CPA treatment. In 73% of cases, the largest peripheral rbet1 objects overlapped by at least 50% of their area with a β-COP–positive object (Supplemental Figure S2E). We can thus estimate that at a minimum, 71% of the largest rbet1 objects are positive for both COPI and ERES markers. This represents a rather conspicuous congruence of COPI and ERES markers with the enlarged rbet1-labeled structures. Due to the relative lack of CPA effect on ERES markers in combination with the close association of the enlarged objects with both COPI and ERES, the most likely identity of the expanded objects are the post-ER, pre-Golgi carriers known as VTCs, elements of the ERGIC. However, electron microscopy analysis is required to distinguish whether the enlarged anterograde structures are physically distinct from versus still connected to ERES.

A recent report by Amodio *et al.* (2009) highlighted the accumulation of anterograde cargo and vesicle machinery in the ER and ERES upon 2-h thapsigargin treatment in the presence of normal extracellular Ca^{2+}. Furthermore, these experiments documented multiple stress-induced morphological changes such as Golgi fragmentation that were not present in the present studies. Because the Amodio conditions would have resulted in very high and sustained cytosolic Ca^{2+} over a much longer timeframe than in our own experiments, it seems likely that our differing conclusions may represent results of very different experimental conditions.

In conclusion, the experiments of Figures 1 and 2 establish for the first time that luminal Ca^{2+} plays an important role in ER-to-Golgi trafficking organelles. Depletion of luminal Ca^{2+} may cause overactive COPII vesicle fusion and/or defects in sorting/recycling to the ER, resulting in expanded peripheral VTC-like organelles.

Vesicular Ca^{2+} Normally Restrains In Vitro COPII Vesicle Fusion and Contents Mixing

To identify mechanisms by which luminal Ca^{2+} may modulate the structure and function of secretory intermediates,

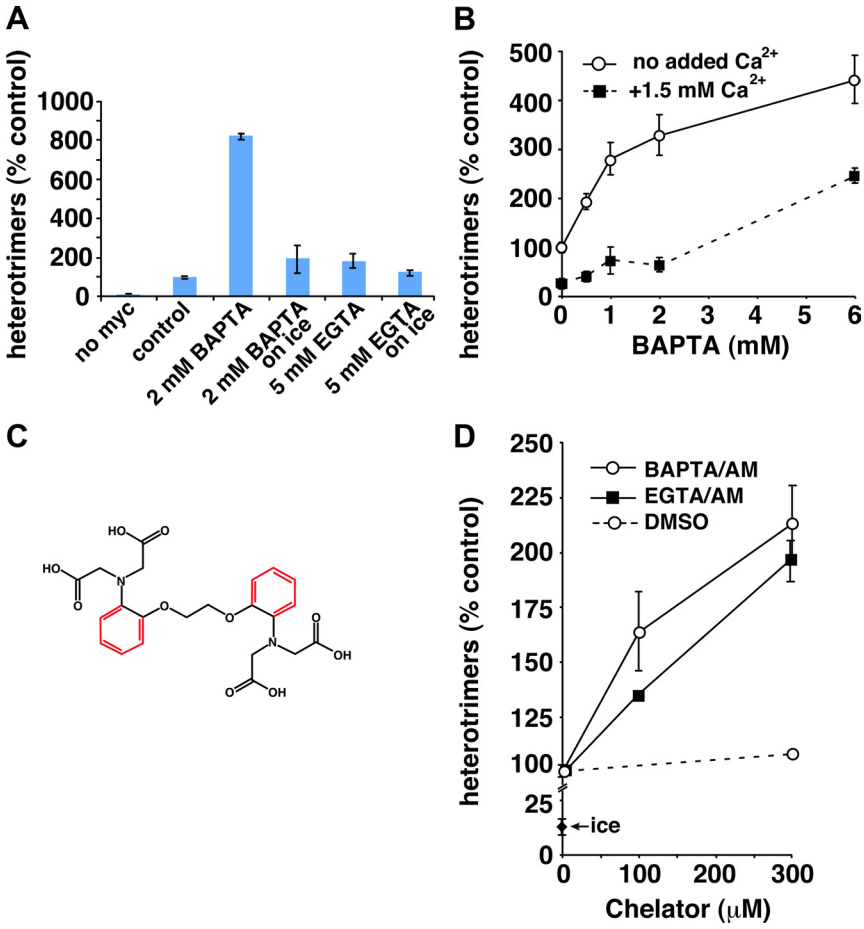

Figure 3. BAPTA, but not EGTA, stimulates COPII vesicle fusion. (A) Homotypic COPII vesicle fusion measured using the in vitro VSV-G heterotrimer cargo mixing assay. The no myc control includes radioactive VSV-G* vesicles, but not VSV-G-myc vesicles, to control for the specificity of the anti-myc immunoprecipitation. BAPTA and EGTA were included in fusion reactions at the indicated concentrations. The on ice reactions had the indicated chelators added after the fusion incubation, before detergent solubilization, to control for possible nonfusion-related effects of the chelators. (B) Titration of fusion reactions with BAPTA in the presence and absence of excess free Ca^{2+}. Because the BAPTA stimulation curve is pushed to the right, it seems that only free BAPTA, and not the Ca^{2+}-bound chelator, has a stimulatory effect on heterotrimer formation. (C) Structures of EGTA (black) and BAPTA (black plus red). (D) Effects of aminomethoxy (/AM) derivatives of BAPTA and EGTA on homotypic COPII vesicle fusion. Both /AM esters were able to partially mimic the effects of BAPTA, suggesting that the selective effects of BAPTA were due to its ability to rapidly chelate escaping luminal Ca^{2+}. Fusion assay data are presented as means of duplicate determinations with error bars representing SE where larger than symbol size.

we used an established cell-free reconstitution of homotypic COPII vesicle fusion (Xu and Hay, 2004; Bentley *et al*., 2006; Yu *et al*., 2006; Cai *et al*., 2007). COPII vesicles generated in vitro from permeabilized NRK cells possess or recruit all components necessary for efficient tethering and fusion to generate pre-Golgi intermediates resembling cellular VTCs (Xu and Hay, 2004). Membrane fusion and contents mixing is scored biochemically by the heterotrimerization of radioactive VSV-G* with nonradioactive VSV-G-myc present initially in distinct COPII vesicle populations. Heterotrimers are easily assayed by detergent solubilization of vesicles, immunoprecipitation using anti-myc antibodies, and autoradiography to detect the radioactive subunits (Xu and Hay, 2004). It has been speculated that luminal Ca^{2+} would most likely affect membrane trafficking at the cytoplasmic surface of membranes after its efflux by regulated or nonspecific processes (Wahl *et al*., 1992; Camello *et al*., 2002; Burgoyne and Clague, 2003; Hay, 2007). As shown in Figure 3A, addition of the fast, membrane-impermeant Ca^{2+} chelator BAPTA resulted in stimulation of heterotrimer production by as much as eightfold (Figure 3A, pos. vs. 2 mM BAPTA). Among different experiments, the stimulation ranged from three- to eightfold over the unstimulated control. The increase in heterotrimers was not solely due to an effect of BAPTA on heterotrimer stability in solution or recovery by immunoprecipitation, because BAPTA stimulated in a time-dependent manner during the fusion reaction (see below; Figure 6) and because addition of BAPTA to fusion reactions on ice, after the fusion reaction but before detergent addition, did not recapitulate the effect (Figure 3A, 2 mM BAPTA, on ice). Finally, a much slower chelator of similar affinity for Ca^{2+}, EGTA, did not stimulate like BAPTA, even at higher concentrations (Figure 3A, 5 mM EGTA). The stimulation of fusion by BAPTA suggests that Ca^{2+} normally suppresses fusion, and this suppression is relieved upon Ca^{2+} chelation.

To test whether the dramatic and unexpected effects of BAPTA on fusion were due to Ca^{2+} chelation as opposed to some other direct action of BAPTA on proteins or membranes, we analyzed the BAPTA sensitivity of fusion in the presence of different bulk free Ca^{2+} concentrations. As shown in Figure 3B, the presence of excess free Ca^{2+} shifted the BAPTA stimulation curve to the right, delaying stimulation until the BAPTA concentration significantly exceeded that of bulk added Ca^{2+}. This indicates that Ca^{2+}-free BAPTA, but not Ca^{2+}-saturated BAPTA, is an active species in our assay and is highly consistent with BAPTA acting, at least in part, through Ca^{2+} chelation. Importantly, it rules out most nonspecific effects that could be caused by high concentrations of this molecule.

The structures of BAPTA and EGTA are shown in Figure 3C. Although these two chelators buffer Ca^{2+} to approximately the same levels at equilibrium, under typical experimental conditions BAPTA reaches equilibrium and thus neutralizes a cellular Ca^{2+} gradient >1000-fold faster than EGTA (Burgoyne and Clague, 2003, and references therein). Taking into account the estimated diffusion rate of Ca^{2+} in cytosol, this may mean that EGTA can never neutralize Ca^{2+} gradients within ≤20 nm of an active egress site, whereas BAPTA can. Hence, selectivity of BAPTA over EGTA has in

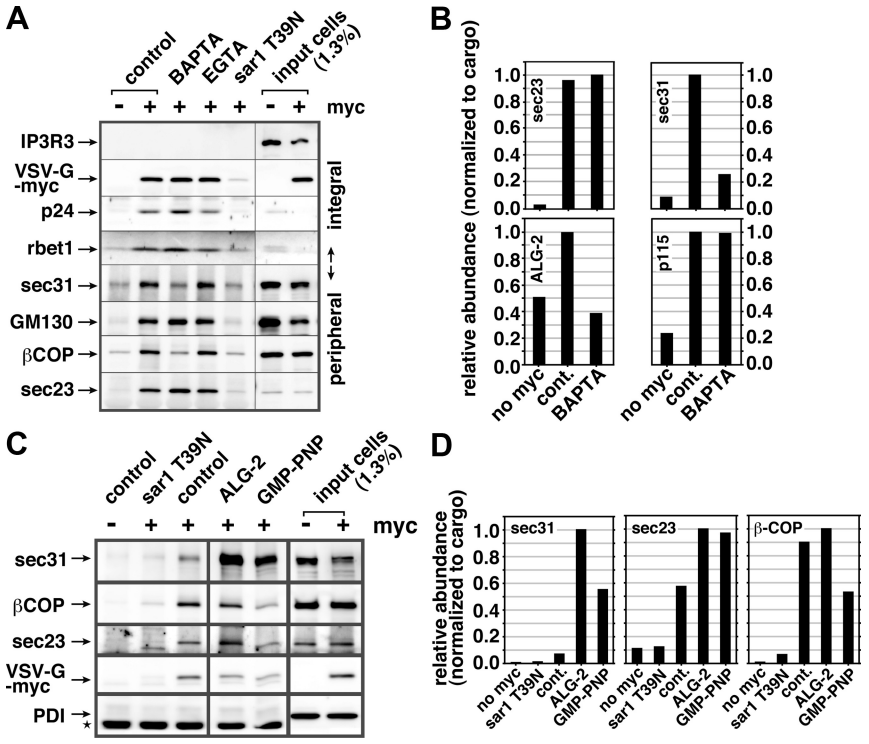

Figure 4. Luminal Ca^{2+} and ALG-2 regulate the retention of select coat subunits on pre-Golgi fusion intermediates. (A) BAPTA specifically extracts select COPI and COPII subunits from forming pre-Golgi intermediates. Homotypic fusion in vitro assays were conducted in the absence or presence of 2 mM BAPTA or EGTA (indicated above), and immunoisolated using anti-myc antibodies. Vesicles were generated from VSV-G-myc transfected cells (+) or nontransfected cells (−) to demonstrate specificity of isolation. In addition, 1 μM purified sar1 T39N was included during the budding stage to demonstrate that the isolated intermediates are COPII derived. Immunoblotted proteins are indicated along left edge. IP3R3, a resident ER membrane protein, additionally demonstrates specificity of budding. (B) Quantitation of a similar immunoisolation experiment (see blot in Supplemental Figure S3). In this experiment, it can be seen that peripheral membrane protein ALG-2 is also sensitive to BAPTA, but p115 is not. (C) Similar immunoisolation experiment where purified ALG-2 is present during the fusion experiment. ALG-2 caused a dramatic retention of outer shell component sec31 but not the COPI component β-COP. The absence of ER resident luminal protein PDI demonstrates specificity of the intermediates isolated. A star indicates the position of cross-reactive antibody heavy chain bands. GMP-PNP shows an estimate of components present on a fully coated vesicle as opposed to components remaining on tethered/fused pre-Golgi intermediates (D) Quantitation of experiment from C. For quantitations (B and D), band intensities were normalized to the recovery of cargo VSV-G-myc in each condition before plotting them on a relative scale with the highest recovery set to 1. Differences in band intensities seen in the input cells lanes (A) were caused by using slightly denser cell suspensions for the nontransfected cell controls.

most cases been interpreted to indicate that the Ca^{2+} sensor/effector mechanism is either very rapid and/or very close to the source of Ca^{2+}, most likely a channel (Burgoyne and Clague, 2003; Hay, 2007). One could even postulate that Ca^{2+} constitutively leaking from the lumen of secretory intermediates could create a steady-state region of elevated Ca^{2+} near the membrane that could persist in EGTA but not in BAPTA (Hay, 2007). If neutralization of Ca^{2+} gradients is involved in the BAPTA stimulation of our fusion assay, then the source of the active Ca^{2+} may be the vesicle lumen. Furthermore, functional chelation of Ca^{2+} at the source should not require an especially fast chelator. To test this possibility, we analyzed the effects of the membrane-permeant aminomethoxy ester derivatives of BAPTA and EGTA, BAPTA/aminomethoxy (AM) and EGTA/AM. As shown in Figure 3D, both membrane-permeant derivatives comparably stimulated the heterotrimer assay at concentrations up to 0.3 mM. Unfortunately, we were unable to interpret results at higher concentrations—hydrolysis of these compounds in cytosol can generate formaldehyde and acetic acid—perhaps explaining why both chelators inhibited our assay at millimolar concentrations (data not shown). The partial recapitulation of the BAPTA stimulatory effect by both EGTA/AM and BAPTA/AM (Figure 3D) but not by EGTA (Figure 3A) is highly consistent with the interpretation that it is the egress of luminal Ca^{2+} that normally has a suppressive effect on COPII vesicle fusogenicity.

Ca^{2+} and ALG-2 Promote Retention of COPII Coat Components on Pre-Golgi Intermediates

To gain more insight into the molecular mechanisms by which vesicular Ca^{2+} regulates VTC morphology and fusion, we analyzed nascent pre-Golgi intermediates for the presence of several peripheral membrane proteins that could potentially affect fusion efficiency. After in vitro tethering/fusion reactions with no chelator, BAPTA, or EGTA, intact pre-Golgi intermediates containing VSV-G-myc cargo were immunoisolated using anti-myc antibody and subjected to immunoblotting. As shown in Figure 4A, the integral membrane components VSV-G-myc, p24 and rbet1, demonstrate the specificity of the immunoisolation (control − vs. control +; also note enrichment in the isolated fractions relative to starting material). Furthermore, the specificity of COPII-dependent budding is demonstrated by the lack of ER resident proteins (IP3 receptor in A, and PDI in C), and by the inhibition of specific product when purified sar1 T39N was included at the budding stage (sar1 T39N). The yield of vesicles seemed to be slightly higher in the BAPTA-treated samples as judged by the band intensities of all three integral membrane proteins. When the same blot was probed for peripheral membrane proteins, two patterns emerged. The golgins GM130 (A) and p115 (B), and the COPII inner shell component sec23 (A and B), seemed to generally follow the recovery of the integral membrane proteins, indicating that the chelators did not significantly change their abundance on membranes. In stark contrast, the COPII outer shell component sec31, as well as the COPI subunit βCOP, were extracted to background levels by BAPTA and were not affected by EGTA. The completeness and specificity of this depletion was reproduced in numerous experiments. These data parallel the functional impact of BAPTA and EGTA on fusion and suggest that residual coats could suppress fusion as effectors of luminal Ca^{2+}.

These experiments also reveal a semiquantitative picture of residual COPII coat retention during homotypic COPII vesicle tethering/fusion in vitro. The experiment shown in Figure 4C and quantified in Figure 4D included a GMP-PNP condition in which this nonhydrolyzable GTP analogue was present from the outset of budding and then throughout the tethering/fusion reaction. By preventing GTP hydrolysis on sar1, GMP-PNP locks the coat onto COPII vesicles (Barlowe *et al*., 1994) and is used here as a standard to represent the components of a fully coated vesicle. Note the dramatic difference between inner and outer shell retention on tethered/fused pre-Golgi intermediates and fully coated vesicles. Normal tethered/fused intermediates possess >55% of the inner shell component sec23 compared with GMP-PNP vesicles (Figure 4D, middle, cont. vs. GMP-PNP). In Cai *et al*. (2007), a similar experiment produced a value of 58%. Thus, the inner shell is relatively stably associated after budding—the ~55% could easily be an underestimate due to coat loss during washing of immunoisolates. In contrast, the outer shell component sec31 is recovered in tethered/fused intermediates at only ~15% of its GMP-PNP value (Figure 4D, left, cont. vs. GMP-PNP). This number varies between experiments to as low as 6%. Hence, the outer shell can be shed independently of the inner shell and remains at much smaller fractions during tethering/fusion and then rigorous washing of immunoisolates. We do not know a precise value for fractional coat retention required to have a regulatory consequence on tethering and fusion. However, a fully coated vesicle contains so much coat protein that it exhibits dramatically altered physical and morphological properties; it is easy to imagine that even 15% of the original outer shell would still be a very abundant peripheral membrane protein and could regulate important aspects of vesicle function.

Both COPI and COPII coats have been suggested to be regulated by Ca^{2+}. COPI, which is recruited to our assembling VTCs but is not strictly required for fusion of COPII vesicles with each other (Xu and Hay, 2004), has been demonstrated to require Ca^{2+} for maximal recruitment to Golgi (Ahluwalia *et al*., 2001); no Ca^{2+} sensor molecule has been suggested for COPI. For COPII in contrast, a potential Ca^{2+} sensor is known: ALG-2 is a penta-EF-hand protein present at ERES that seemed to stabilize sec31 on the membrane but was not required for ERES formation or function (Yamasaki *et al*., 2006). We reasoned that ALG-2 could potentially have a dramatic effect on residual vesicle coat retention, because other COPII stabilizing influences present at ERES, such as sar1 guanine nucleotide exchange factor and ERES scaffold proteins would be absent at this stage. We first asked whether ALG-2 was restricted to ERES or whether it was also present on COPII vesicles and their fusion products. ALG-2 is an abundant component of liver cytosol and unfortunately displays high nonspecific binding to surfaces. However, despite a high background in our immunoisolation procedure, there was a definite association of ALG-2 with assembling pre-Golgi intermediates (Figure 4B, bottom left, no myc vs. control; unquantified blot shown in Supplemental Figure S3). Furthermore, the specific ALG-2 signal was removed by BAPTA treatment, consistent with ALG-2 regulating coat retention as a function of Ca^{2+} (Figure 4B, bottom left, control vs. BAPTA).

If, as suggested above, ALG-2 regulates coat retention on pre-Golgi intermediates, then increased ALG-2 should cause excessive coat retention. This was tested using purified recombinant ALG-2 in the COPII vesicle assembly assay/immunoisolation. As shown qualitatively in Figure 4C and quantitatively in Figure 4D, addition of 1 μM ALG-2 to COPII vesicle fusion assays led to a dramatic increase in sec31 retention on VSV-G-myc–containing intermediates. The increase in abundance of sec31 was >10-fold over control sec31 retention and even increased approximately twofold greater than that caused by inclusion of GMP-PNP (Figure 4D, left, cont. vs. ALG-2). This increase in the COPII outer shell occurred mostly independently of the inner shell component sec23, whose abundance increased less than twofold (Figure 4D, middle, cont. vs. ALG-2). Also note that ALG-2 did not affect the abundance of COPI component βCOP (Figure 4D, right, cont. vs. ALG-2). This suggests that COPI is recruited to and stabilized to pre-Golgi intermediates by a completely independent Ca^{2+}-dependent mechanism.

In summary, Figure 4 demonstrates that Ca^{2+} stabilizes components of both COPII and COPI on pre-Golgi intermediate membranes. For COPII, the mechanism of stabilization can involve the Ca^{2+} sensor ALG-2, which primarily stabilizes the COPII outer shell. Modulation of residual outer shell COPII coat components by ALG-2 could potentially provide a mechanism by which luminal Ca^{2+} affects the structure and function of VTCs in cells (Figures 1 and 2) and by which vesicle-associated Ca^{2+} suppresses homotypic COPII vesicle fusion in vitro (Figure 3).

ALG-2 Regulates In Vitro COPII Vesicle Contents Mixing in a Ca^{2+}-dependent Manner

Despite a clear effect of ALG-2 and Ca^{2+} on the quantity of sec31 at ERES, a functional effect on vesicle budding was not observed (Yamasaki *et al*., 2006). We wondered whether Ca^{2+}-dependent retention of sec31 by ALG-2 might be more functionally rate limiting at a postbudding step. To test this possibility directly, we added purified recombinant GST-ALG-2 or GST to tethering/fusion reactions and monitored fusion using the VSV-G heterotrimer assay. As shown in Figure 5A, GST-ALG-2 potently inhibited COPII vesicle fusogenicity in a dose-dependent manner, with maximal inhibition achieved by 1 μM protein. To test whether ALG-2 inhibition of fusion required Ca^{2+} binding capacity, we added GST-ALG-2 E47,114A, a mutant in which two EF-hands are disrupted and which exhibits dramatically reduced Ca^{2+} binding (Lo *et al*., 1999). The inhibitory properties of this protein were greatly reduced, suggesting that the wild-type protein uses Ca^{2+} binding to exert its inhibitory effect. The recombinant proteins, which were expressed and purified at equivalent abundance and solubility, are shown in Figure 5B.

To further explore the relationship between ALG-2, vesicular Ca^{2+}, and BAPTA, we tested the inhibitory properties of ALG-2 in the presence and absence of BAPTA. As can be seen in Figure 5C (left), in the absence of BAPTA, we used a dose of GST-ALG-2 that inhibited fusion by ~50%. As before, the same concentration of the E47,114A mutant inhibited only slightly. We also included anti-syntaxin 5 antibody at a concentration that inhibits fusion by ~50% as well. This antibody has been well characterized as an inhibitor of in vitro fusion assays (Williams *et al*., 2004; Xu and Hay, 2004; Bentley *et al*., 2006); at the concentration used here, fusion is partially inhibited but not tethering (Bentley *et al*., 2006). In Figure 5C (right), the same inhibitors were tested in the presence of BAPTA during the same experiment, leading to several observations. First, the Ca^{2+}-dependent component of ALG-2 inhibition is effectively negated—wild-type and E47,114A mutant inhibit to approximately the same small degree. This indicates that Ca^{2+} chelation by BAPTA completely reverses the mechanism by which ALG-2 inhibits fusion, consistent with that mechanism being stabilization of sec31, which BAPTA extracts from membranes. Second, the

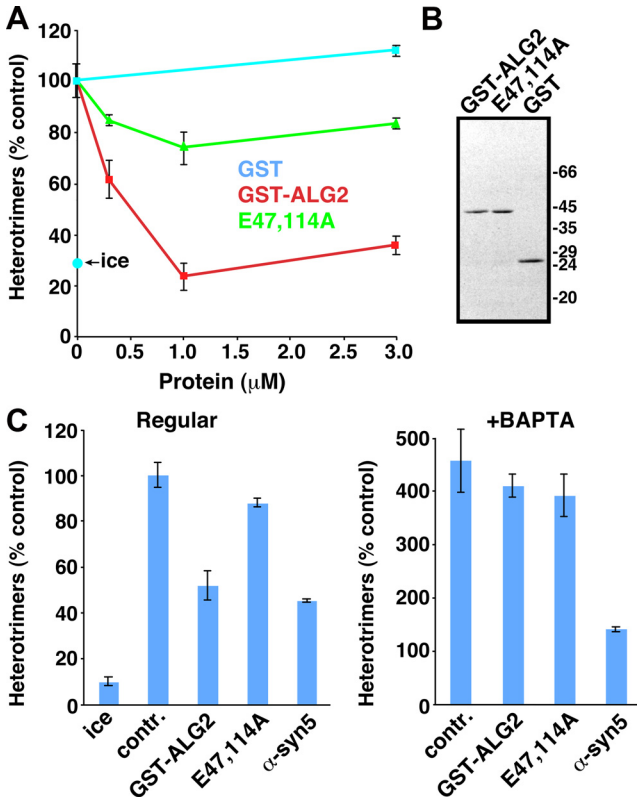

Figure 5. ALG-2 regulates in vitro COPII vesicle homotypic fusion in a Ca^{2+}-dependent manner. (A) Homotypic COPII vesicle fusion measured using the in vitro VSV-G heterotrimer cargo mixing assay. Purified GST, GST-ALG-2 wild-type, or GST-ALG-2 E47,114A mutant proteins were included in fusion incubations at the indicated concentrations. The ice control includes radioactive VSV-G* vesicles and VSV-G-myc vesicles, but the low temperature prevents a specific fusion signal. (B) PAGE gel on purified proteins used in A and C, stained with Coomassie Blue. Proteins were used in fusion assays in the same proportions as on the gel. (C) Fusion experiment using partially inhibitory doses of the proteins indicated along the bottom. The left panel experiment was conducted in the absence of BAPTA. The right panel experiment was conducted, in the same experiment, in the presence of 2 mM BAPTA. Fusion values for both panels are normalized to the positive control signal in the absence of BAPTA (set to 100%). BAPTA negates the specific inhibitory effect of GST-ALG-2 but not that of anti-syntaxin 5 antibody. Fusion assay data are presented as means of duplicate determinations, with error bars representing SE where they are larger than symbol size.

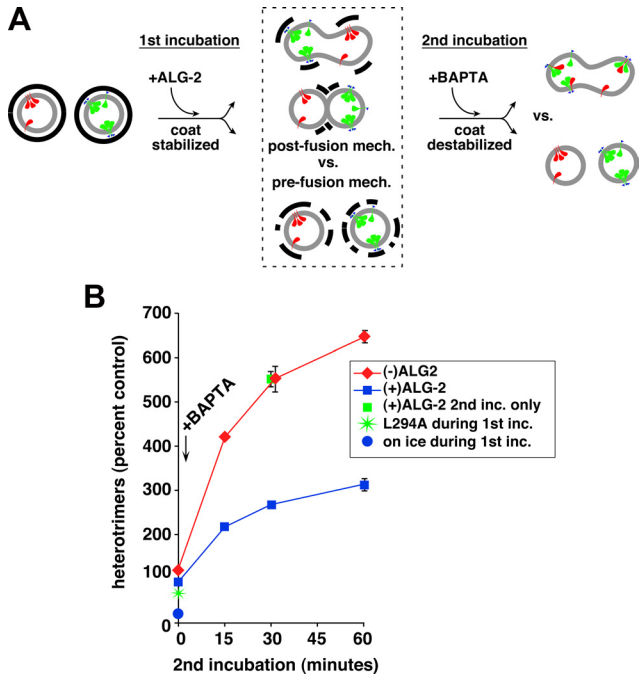

Figure 6. ALG-2–dependent coat retention primarily inhibits via a prefusion mechanism. (A) Outline of experiment to distinguish between pre- or postfusion mechanisms by which ALG-2 inhibits heterotrimer assay (see text for explanation). Cargos VSV-G-myc and radioactive VSV-G* are depicted in green and red, respectively. COPII coat is represented by thick black lines. (B) Heterotrimer data from experiment depicted in A. Heterotrimers are normalized with 100% representing the amount produced during the first incubation in the absence of recombinant ALG-2, before addition of BAPTA and second incubation. BAPTA was omitted from the conditions plotted at time 0; BAPTA was added to all other conditions, while on ice, just before beginning the second incubation at 32°C. ALG-2 added during the first incubation had a dramatic consequence on the subsequent heterotrimer signal (red vs. blue lines), but ALG-2 added only during the second incubation had no influence (green square). Plotted are means of duplicate reactions, with error bars to represent SE where they exceeded symbol size.

BAPTA-dependent fusion signal is still largely sensitive to anti-syntaxin 5 antibody, indicating that SNARE-dependent membrane fusion is required for the BAPTA stimulation of heterotrimer formation. In summary, the experiments in Figure 5 demonstrate that ALG-2, through Ca^{2+}-dependent stabilization of the COPII outer shell, can restrain membrane fusion or membrane mixing (see below). Thus, ALG-2 is a very good candidate to mediate the effects of luminal Ca^{2+} on VTC morphology and size (Figures 1 and 2) and to mediate the suppression of fusogenicity relieved by BAPTA (Figures 3 and 5).

ALG-2 Inhibits Heterotrimerization via a Prefusion Mechanism

Although the heterotrimer assay strictly depends upon membrane fusion, there are actually two fundamentally distinct mechanisms by which ALG2-dependent residual coat retention could affect the fusion signal. As diagrammed in Figure 6A, dashed box area, residual COPII stabilization could either 1) act via a prefusion mechanism by inhibiting close vesicle approach, fusion machinery availability, and/or docking (bottom intermediate in the dashed box); or 2) limit postfusion membrane mixing by maintaining membrane microdomains that prevent mixing of cargo from fused or hemifused vesicles (top outcome). Although the outer shell does not directly bind cargo, its presence could affect cargo mixing by binding and immobilizing the cargo-bound inner shell. It could also sterically prevent the conversion from hemifusion to full fusion by limiting membrane flow into the fusion pore. Importantly, the two very distinct mechanisms outlined are not mutually exclusive and either could potentially exert a strong impact on pre-Golgi intermediates under different conditions. To distinguish between prefusion and postfusion inhibition by ALG-2, we performed the experiment diagrammed in Figure 6A. A first fusion incubation was performed in the presence of a partially inhibitory concentration of recombinant ALG-2 to stabilize the COPII outer shell. The first incubation should result in intermediates depicted in the dashed box; the second incubation will distinguish which are predominant. During the second incubation, BAPTA

will be present to reverse ALG-2 stabilization of the COPII coat, a manipulation suggested by the known ability of BAPTA to negate ALG-2 inhibition (Figure 5C). This second incubation will freely permit late events in our assay such as the completion of membrane mixing and heterotrimerization, but it will be biased against early steps in membrane fusion for two reasons: 1) first, membrane fusion in this assay generally reaches a maximum after 1 h (the length of the first incubation), presumably as needed components are exhausted (Supplemental Figure S4); and 2) we added α-soluble N-ethylmaleimide-sensitive factor attachment protein (α-SNAP) L294A, a dominant-negative inhibitor of *N*-ethylmaleimide sensitive factor-dependent SNARE recycling, during the second incubation to inhibit the availability of free SNAREs for new rounds of fusion (Bentley *et al*., 2006). If ALG-2 inhibited via a postfusion mechanism, the final outcome after the second incubation would be that of unimpaired heterotrimerization (Figure 6A, top right outcome). However, if ALG-2 inhibits via largely prefusion mechanisms, the inability to support new rounds of fusion during the second incubation should result in a permanent inhibition of heterotrimerization (Figure 6A, bottom right outcome).

Figure 6B shows heterotrimer formation over time during the second stage incubation. When vesicles were first incubated without ALG-2, and then incubated with BAPTA, a rapid and robust amplification approaching sevenfold of the heterotrimer signal was obtained (red line). In stark contrast, the vesicles that had been incubated with ALG-2 during the first incubation were severely hampered for heterotrimer formation, reaching an apparent maximum at threefold stimulation. Importantly, ALG-2 influenced the experiment only during the first incubation, because addition of ALG-2 along with BAPTA only during the second incubation reached a similar maximum as BAPTA alone (Figure 6B, green square symbol at 30 min). The inability of ALG-2–preincubated vesicles to recover a robust fusion signal in the presence of BAPTA implies that ALG-2–dependent coat retention inhibits largely at an early, prefusion stage of the assay, for example SNARE-dependent docking. On the other hand, the ability of BAPTA to robustly stimulate heterotrimerization of the control vesicles during the second incubation implies that under basal conditions, the ~10% of residual sec31 must limit later stages in fusion or postfusion events. The experiment in Figure 3C does not define a precise stage at which BAPTA stimulates other than that it seems to be later than the prefusion stage at which ALG-2 inhibits (see *Discussion*). In total, the experiment demonstrates that ALG-2–dependent coat retention inhibits homotypic COPII vesicle fusion at a prefusion step, and implies that different degrees of coat retention may inhibit different stages of fusion and membrane mixing.

DISCUSSION

Our results include the somewhat surprising finding that Ca^{2+} suppresses membrane fusion in the early secretory pathway. This contrasts with several other membrane trafficking steps, such as regulated exocytosis, endosome fusion, and intra-Golgi transport, where a stimulatory role for Ca^{2+} has been documented (for reviews, see Burgoyne and Clague, 2003; Hay, 2007). We can only speculate that ER-to-Golgi transport represents an ideal opportunity for cellular machinery to use luminal Ca^{2+} in a complex, graded, opportunistic manner. The ER normally contains a very high free Ca^{2+} concentration (Supplemental Figure S1B, 386 μM in living NRK cells); because SERCA pumps are retained in the ER and do not enter COPII vesicles, it is assumed that nonspecific leak causes free luminal Ca^{2+} in secretory intermediates to progressively decrease as they mature through the intermediate compartment (Pezzati *et al*., 1997). Thus, the ever-changing Ca^{2+} signature of pre-Golgi intermediates could be used in a manner not yet appreciated at other transport steps. For example, the high luminal Ca^{2+}, and thus Ca^{2+} leak, from the ER and newly formed COPII vesicles would tend to discourage back-fusion of COPII vesicles with the donor compartment, simultaneously favoring their fusion with more mature, functional VTCs exhibiting lower Ca^{2+} signatures and discouraging premature fusion with the Ca^{2+}-rich Golgi. This would enforce an ordered directionality to COPII vesicle fusions. On the other hand, should an abundance of cargo dictate a dramatic increase in vesicle budding beyond the acceptor capacity of pre-existing, mature VTCs, the primary vesicles' prolonged dwell time near ERES would eventually result in lower Ca^{2+} signatures and greater homotypic fusion of primary vesicles to generate nascent VTCs. This homeostatic mechanism could thus enforce efficient forward movement of cargo through preexisting secretory and sorting intermediates, yet also represent a means to dictate new VTC biogenesis when excessive cargo loads dictate. By the time mature VTCs reach the Golgi area, they may be nearly depleted of free luminal Ca^{2+}; yet, Golgi Ca^{2+} ATPases maintain high luminal Ca^{2+} within Golgi cisternae themselves. Hence, the documented requirement for Ca^{2+} for fusion of pre-Golgi intermediates with the Golgi (Beckers and Balch, 1989) and fusion within the Golgi (Porat and Elazar, 2000) would direct the ordered fusion of mature VTCs with an appropriate high Ca^{2+} acceptor compartment. The differing responses to Ca^{2+}, suppressive (near ER exit sites) versus stimulatory (near the Golgi), could be dictated by differing accessory trafficking proteins, such as ALG-2, that may be recruited to and lost from maturing secretory intermediates in a stage-specific manner.

Depletion of luminal Ca^{2+} caused dramatic changes in the organization of the ER-Golgi intermediate compartment (Figures 1 and 2), recruitment of trafficking machinery to pre-Golgi intermediates (Figure 4), and rates of homotypic COPII vesicle fusion (Figures 3, 5, and 6). These changes may affect the efficiency of anterograde trafficking. We also anticipate that the rearrangements caused by luminal Ca^{2+} depletion should affect the efficiency of cargo sorting, another primary function of VTCs. The overall morphology and size of VTCs is probably a determining factor of both their transport and sorting capacity. However, Ca^{2+}-dependent residual coat retention could present a more direct mechanism by which sorting capacity could be regulated. The presence of Ca^{2+}-stabilized residual COPII coat on pre-Golgi intermediates could create membrane microdomains within which cargo from different vestigial vesicles remains relatively restricted. This would potentially allow anterograde cargo to remain relatively concentrated in certain regions of VTCs, forcing the other, noncoated, regions to accumulate extra membrane and escaped ER proteins and machinery for more efficient return to the ER. VTCs are perhaps the most active sorting station of the secretory pathway; indeed, the majority of membrane exported from the ER in COPII vesicles seems to be retrieved during the process of VTC maturation and cargo concentration (Martínez-Menárguez *et al*., 1999). Powerful new techniques that combine high pressure freezing, three-dimensional electron tomography, and immunolabeling have continued to support the finding that >70% of COPII labeling around ERES is present on free vesicles and dumbbell-shaped tubules not physically continuous with the ER (Zeuschner *et al*., 2006).

This is strong evidence for residual COPII proteins remaining on (or else rebinding to) membranes after budding, tethering, and possibly even fusion. Unfortunately, our experiments do not yet definitively indicate whether residual COPII coat remains after homotypic vesicle fusion. Although our experiments demonstrate the ability of BAPTA to stimulate at a very late stage in the in vitro assay (Figure 6B, red line) and thus imply postfusion membrane mixing effects of residual coat, the mechanism of BAPTA action is not completely understood (see below) and our bulk immunoisolates of nascent VTCs do not unambiguously prove the existence of sec31 on a fused structure, per se. On the other hand, our experiments using ALG-2 at least prove that residual outer shell can remain long enough to regulate at a prefusion stage. The functional impacts of residual COPII coat during VTC biogenesis may occur at different stages in tethering, docking, fusion, and even postfusion mechanisms. The decreasing luminal Ca^{2+} signature of maturing VTCs has also been suggested to play a direct role on sorting via the activity of cargo receptors such as ERGIC-53 (Appenzeller-Herzog *et al*., 2004).

The precise relationship between luminal Ca^{2+} and the mechanism of BAPTA action (Figures 3–6) remains somewhat speculative. The functional selectivity of BAPTA over EGTA, and the partial reproduction of the effects of BAPTA by EGTA/AM are consistent with leaking luminal Ca^{2+}, very near the site of membrane fusion, as the functionally relevant Ca^{2+}. The ability of BAPTA to aggressively neutralize spatially restricted and fleeting Ca^{2+} gradients has been the conventional explanation for BAPTA's selectivity in many cell systems (see Burgoyne and Clague, 2003, and references therein). However, we were unable to mimic BAPTA using Ca^{2+} ionophores such as A23187 or ionomycin (data not shown), suggesting that the functionally relevant Ca^{2+} pool was resistant to these conditions. The relevant Ca^{2+} pool may persist in the presence of ionophores; for example it may be tightly membrane associated in such a manner that BAPTA, which contains aromatic rings that could potentially interact with membranes (Figure 3C), is a uniquely functional chelator. It is also possible that BAPTA simply chelates free cytosolic Ca^{2+} to lower equilibrium levels than EGTA under biological conditions, despite their apparently equal Ca^{2+} affinities. That the effects of BAPTA are related to Ca^{2+} chelation is strongly supported by our data: 1) excess Ca^{2+} neutralizes the ability of BAPTA to stimulate fusion (Figure 3B); 2) a structurally distinct hydrophobic chelator EGTA/AM, but not the hydrophilic EGTA, can partially mimic the effect (Figure 3D); 3) BAPTA specifically extracts coat components sec31 and β-COP previously shown to be stabilized by Ca^{2+} on the membrane (Figure 4) and the EF-hand protein ALG-2 causes opposite effects (Figures 4 and 5). That BAPTA stimulates our fusion assay through a bona fide fusion mechanism is also clear, because it causes very little increase in heterotrimers in the presence of anti-syntaxin 5 antibody (Figure 5C). The precise relationship between luminal Ca^{2+} pools, ALG-2 and the functionally selective effects of chelators remain to be fully explained.

ALG-2 has been implicated in the Ca^{2+}-dependent stabilization of sec31 at ERES, but no consequences of ALG-2 on ERES function have yet to be demonstrated (Yamasaki *et al*., 2006; la Cour *et al*., 2007; Shibata *et al*., 2007). It is interesting to speculate that the lack of ALG-2 effects on vesicle budding may have been because ALG-2's most limiting function occurs later in the pathway, during vesicle targeting and fusion. Other ERES machinery may provide sufficient stabilization of sec31 for budding purposes. Later, after GTP hydrolysis by sar1 and in the absence of ERES scaffolding proteins, ALG-2 may play a much more limiting role in maintaining microdomains of COPII coat on vesicles for the purpose of regulating fusion and/or sorting (Figures 5 and 6). However, the details of how ALG-2 may do this remain sketchy. PEF proteins such as ALG-2 seem to exist either as homodimers or heterodimers with another PEF protein (Maki *et al*., 2002); for example, ALG-2 can exist as a homodimer or as a heterodimer with the PEF protein peflin (Kitaura *et al*., 2001; Okumura *et al*., 2009). The PEF homo- or heterodimer may then cross-bridge two ligand molecules in a Ca^{2+}-dependent manner. For example, ALG-2 mediates a Ca^{2+}-dependent complex between alix and tsg101, two proteins involved in multivesicular body biogenesis (Okumura *et al*., 2009). Based upon this precedent, we might expect that ALG-2 on pre-Golgi intermediates is cross-bridging sec31 either to itself or to another, more stably membrane associated binding partner. We do not know what this other ALG-2 receptor on COPII-derived vesicles may be, although a luminal Ca^{2+} conducting protein would be a tantalizing possibility that would fit with the chelator selectivity of our effects. ALG-2 had a much greater impact on sec31 retention than retention of sec23 (Figure 4, C and D). Our speculation would be that the COPII inner shell is maintained on the membrane primarily through interaction with vesicle cargo, whereas the outer shell, sec31, requires Ca^{2+}-dependent interactions with ALG-2 for stabilization. One commonality of PEF proteins is their interaction with proline motifs of the target proteins. Indeed, ALG-2 interacts with a proline-rich region of sec31 (Yamasaki *et al*., 2006). Because sec23 also interacts with the proline-rich domain of sec31 (Shaywitz *et al*., 1997; Bi *et al*., 2007), it is even possible that ALG-2 binds mutually exclusively with sec23—effectively forcing sec31 from an inner shell-, cargo-, and sar1-dependent membrane association into an ALG-2– and Ca^{2+}-dependent mode of association. One challenge in nailing down functions of the PEF proteins is their potential redundancy. Whether other members of the PEF family such as the closely related peflin protein could in part compensate for ALG-2 depletion is not known. Despite strong evidence for ALG-2 involvement in diverse cellular functions, ALG-2 knockout animals have had few visible defects. Indeed, we have so far observed no dramatic rearrangements of VTCs or ERES upon ~90% ALG-2 knockdown in NRK cells (data not shown). Multiple knockdowns and/or dominant-negative approaches may be required to provide absolute proof of the significance of ALG-2 to the COPII biosynthetic secretory pathway.

ACKNOWLEDGMENTS

We thank Dr. Scott Wetzel for the valuable advice regarding image quantitation and Dr. Meg Trahey for critical comments on the manuscript. We also thank Anna Schreilechner for excellent technical assistance and Prof. Dr. R. Tsien (University of California–San Diego) for YC2.1, YC3.6, and D1ER. This research was supported by National Institutes of Health grant R01 GM-059378 (to J.C.H.) and Austrian Science Funds (Fonds zur Förderung der wissenschaftlichen Forschung, P20181-B05 and F3010-B05; to W.F.G.). Work at the University of Montana benefited from a highly supportive environment provided by National Institutes of Health COBRE Center grant P20 RR015583.

REFERENCES

Ahluwalia, J. P., Topp, J. D., Weirather, K., Zimmerman, M., and Stamnes, M. (2001). A role for calcium in stabilizing transport vesicle coats. J. Biol. Chem. *276*, 34148–34155.

Allan, B. B., Moyer, B. D., and Balch, W. E. (2000). Rab1 recruitment of p115 into a cis-SNARE complex: programming budding COPII vesicles for fusion. Science *289*, 444–448.

Alvarez, C., Garcia-Mata, R., Hauri, H. P., and Sztul, E. (2001). The p115-interactive proteins GM130 and giantin participate in endoplasmic reticulum-Golgi traffic. J. Biol. Chem. *276*, 2693–2700.

Amodio, G., Renna, M., Paladino, S., Venturi, C., Tacchetti, C., Moltedo, O., Franceschelli, S., Mallardo, M., Bonatti, S., and Remondelli, P. (2009). Endoplasmic reticulum stress reduces the export from the ER and alters the architecture of post-ER compartments. Int. J. Biochem. Cell Biol. *41*, 2511–2521.

Appenzeller-Herzog, C., Roche, A. C., Nufer, O., and Hauri, H. P. (2004). pH-induced conversion of the transport lectin ERGIC-53 triggers glycoprotein release. J. Biol. Chem. *279*, 12943–12950.

Aridor, M., Bannykh, S. I., Rowe, T., and Balch, W. E. (1995). Sequential coupling between COPII and COPI vesicle coats in endoplasmic reticulum to Golgi transport. J. Cell Biol. *131*, 875–893.

Barlowe, C., Orci, L., Yeung, T., Hosobuchi, M., Hamamoto, S., Salama, N., Rexach, M. F., Ravazzola, M., Amherdt, M., and Schekman, R. (1994). COPII: a membrane coat formed by Sec proteins that drive vesicle budding from the endoplasmic reticulum. Cell *77*, 895–907.

Beckers, C. J., and Balch, W. E. (1989). Calcium and GTP: essential components in vesicular trafficking between the endoplasmic reticulum and Golgi apparatus. J. Cell Biol. *108*, 1245–1256.

Ben-Tekaya, H., Miura, K., Pepperkok, R., and Hauri, H. P. (2005). Live imaging of bidirectional traffic from the ERGIC. J. Cell Sci. *118*, 357–367.

Bentley, M., Liang, Y., Mullen, K., Xu, D., Sztul, E., and Hay, J. C. (2006). SNARE status regulates tether recruitment and function in homotypic COPII vesicle fusion. J. Biol. Chem. *281*, 38825–38833.

Bi, X., Mancias, J. D., and Goldberg, J. (2007). Insights into COPII coat nucleation from the structure of Sec23.Sar1 complexed with the active fragment of Sec31. Dev. Cell *13*, 635–645.

Bonifacino, J. S., and Glick, B. S. (2004). The mechanisms of vesicle budding and fusion. Cell *116*, 153–166.

Burgoyne, R. D., and Clague, M. J. (2003). Calcium and calmodulin in membrane fusion. Biochim. Biophys. Acta *1641*, 137–143.

Cai, H., Yu, S., Menon, S., Cai, Y., Lazarova, D., Fu, C., Reinisch, K., Hay, J. C., and Ferro-Novick, S. (2007). TRAPPI tethers COPII vesicles by binding the coat subunit Sec23. Nature *445*, 941–944.

Camello, C., Lomax, R., Petersen, O. H., and Tepikin, A. V. (2002). Calcium leak from intracellular stores–the enigma of calcium signalling. Cell Calcium *32*, 355–361.

Chen, J. L., Ahluwalia, J. P., and Stamnes, M. (2002). Selective effects of calcium chelators on anterograde and retrograde protein transport in the cell. J. Biol. Chem. *277*, 35682–35687.

Colombo, M. I., Beron, W., and Stahl, P. D. (1997). Calmodulin regulates endosome fusion. J. Biol. Chem. *272*, 7707–7712.

De Haro, L., Quetglas, S., Iborra, C., Lévêque, C., and Seagar, M. (2003). Calmodulin-dependent regulation of a lipid binding domain in the v-SNARE synaptobrevin and its role in vesicular fusion. Biol. Cell *95*, 459–464.

Guan, K. L., and Dixon, J. E. (1991). Eukaryotic proteins expressed in *Escherichia coli*: an improved thrombin cleavage and purification procedure of fusion proteins with glutathione S-transferase. Anal. Biochem. *192*, 262–267.

Hay, J. C. (2007). Calcium: a fundamental regulator of intracellular membrane fusion? EMBO Rep. *8*, 236–240.

Hay, J. C., Klumperman, J., Oorschot, V., Steegmaier, M., Kuo, C. S., and Scheller, R. H. (1998). Localization, dynamics, and protein interactions reveal distinct roles for ER and Golgi SNAREs. J. Cell Biol. *141*, 1489–1502.

Haze, K., Yoshida, H., Yanagi, H., Yura, T., and Mori, K. (1999). Mammalian transcription factor ATF6 is synthesized as a transmembrane protein and activated by proteolysis in response to endoplasmic reticulum stress. Mol. Biol. Cell *10*, 3787–3799.

Hughes, H., Budnik, A., Schmidt, K., Palmer, K. J., Mantell, J., Noakes, C., Johnson, A., Carter, D. A., Verkade, P., Watson, P., and Stephens, D. J. (2009). Organisation of human ER-exit sites: requirements for the localisation of Sec16 to transitional ER. J. Cell Sci. *122*, 2924–2934.

Joglekar, A. P., Xu, D., Rigotti, D. J., Fairman, R., and Hay, J. C. (2003). The SNARE motif contributes to rbet1 intracellular targeting and dynamics independently of SNARE interactions. J. Biol. Chem. *278*, 14121–14133.

Kitaura, Y., Matsumoto, S., Satoh, H., Hitomi, K., and Maki, M. (2001). Peflin and ALG-2, members of the penta-EF-hand protein family, form a heterodimer that dissociates in a Ca2+-dependent manner. J. Biol. Chem. *276*, 14053–14058.

la Cour, J. M., Mollerup, J., and Berchtold, M. W. (2007). ALG-2 oscillates in subcellular localization, unitemporally with calcium oscillations. Biochem. Biophys. Res. Commun. *353*, 1063–1067.

Lo, K. W., Zhang, Q., Li, M., and Zhang, M. (1999). Apoptosis-linked gene product ALG-2 is a new member of the calpain small subunit subfamily of Ca2+-binding proteins. Biochemistry *38*, 7498–7508.

Loh, E., Peter, F., Subramaniam, V. N., and Hong, W. (2005). Mammalian Bet3 functions as a cytosolic factor participating in transport from the ER to the Golgi apparatus. J. Cell Sci. *118*, 1209–1222.

Maki, M., Kitaura, Y., Satoh, H., Ohkouchi, S., and Shibata, H. (2002). Structures, functions and molecular evolution of the penta-EF-hand Ca2+-binding proteins. Biochim. Biophys. Acta *1600*, 51–60.

Malli, R., Frieden, M., Trenker, M., and Graier, W. F. (2005). The role of mitochondria for Ca2+ refilling of the endoplasmic reticulum. J. Biol. Chem. *280*, 12114–12122.

Malli, R., Naghdi, S., Romanin, C., and Graier, W. F. (2008). Cytosolic Ca2+ prevents the subplasmalemmal clustering of STIM *1*, an intrinsic mechanism to avoid Ca2+ overload. J. Cell Sci. *121*, 3133–3139.

Martínez-Menárguez, J. A., Geuze, H. J., Slot, J. W., and Klumperman, J. (1999). Vesicular tubular clusters between the ER and Golgi mediate concentration of soluble secretory proteins by exclusion from COPI-coated vesicles. Cell *98*, 81–90.

Mason, M. J., Garcia-Rodriguez, C., and Grinstein, S. (1991). Coupling between intracellular Ca2+ stores and the Ca2+ permeability of the plasma membrane. Comparison of the effects of thapsigargin, 2,5-di-(tert-butyl)-1,4-hydroquinone, and cyclopiazonic acid in rat thymic lymphocytes. J. Biol. Chem. *266*, 20856–20862.

Mills, I. G., Urbé, S., and Clague, M. J. (2001). Relationships between EEA1 binding partners and their role in endosome fusion. J. Cell Sci. *114*, 1959–1965.

Miyawaki, A., Llopis, J., Heim, R., McCaffery, J. M., Adams, J. A., Ikura, M., and Tsien, R. Y. (1997). Fluorescent indicators for Ca2+ based on green fluorescent proteins and calmodulin. Nature *388*, 882–887.

Moyer, B. D., Allan, B. B., and Balch, W. E. (2001). Rab1 interaction with a GM130 effector complex regulates COPII vesicle cis-Golgi tethering. Traffic *2*, 26.

Nagai, T., Yamada, S., Tominaga, T., Ichikawa, M., and Miyawaki, A. (2004). Expanded dynamic range of fluorescent indicators for Ca(2+) by circularly permuted yellow fluorescent proteins. Proc. Natl. Acad. Sci. USA *101*, 10554–10559.

Okumura, M., Ichioka, F., Kobayashi, R., Suzuki, H., Yoshida, H., Shibata, H., and Maki, M. (2009). Penta-EF-hand protein ALG-2 functions as a Ca2+-dependent adaptor that bridges Alix and TSG101. Biochem. Biophys. Res. Commun. *386*, 237–241.

Osibow, K., Malli, R., Kostner, G. M., and Graier, W. F. (2006). A new type of non-Ca2+-buffering Apo(a)-based fluorescent indicator for intraluminal Ca2+ in the endoplasmic reticulum. J. Biol. Chem. *281*, 5017–5025.

Palmer, A. E., Jin, C., Reed, J. C., and Tsien, R. Y. (2004). Bcl-2-mediated alterations in endoplasmic reticulum Ca2+ analyzed with an improved genetically encoded fluorescent sensor. Proc. Natl. Acad. Sci. USA *101*, 17404–17409.

Peters, C., and Mayer, A. (1998). Ca2+/calmodulin signals the completion of docking and triggers a late step of vacuole fusion. Nature *396*, 575–580.

Pezzati, R., Bossi, M., Podini, P., Meldolesi, J., and Grohovaz, F. (1997). High-resolution calcium mapping of the endoplasmic reticulum-Golgi-exocytic membrane system. Electron energy loss imaging analysis of quick frozen-freeze dried PC12 cells. Mol. Biol. Cell *8*, 1501–1512.

Porat, A., and Elazar, Z. (2000). Regulation of intra-Golgi membrane transport by calcium. J. Biol. Chem. *275*, 29233–29237.

Portzehl, H., Caldwell, P. C., and Rueegg, J. C. (1964). The dependence of contraction and relaxation of muscle fibres from the crab *Maia squinado* on the internal concentration of free calcium ions. Biochim. Biophys. Acta *79*, 581–591.

Presley, J. F., Cole, N. B., Schroer, T. A., Hirschberg, K., Zaal, K. J., and Lippincott-Schwartz, J. (1997). ER-to-Golgi transport visualized in living cells. Nature *389*, 81–85.

Pryor, P. R., Mullock, B. M., Bright, N. A., Gray, S. R., and Luzio, J. P. (2000). The role of intraorganellar Ca(2+) in late endosome-lysosome heterotypic fusion and in the reformation of lysosomes from hybrid organelles. J. Cell Biol. *149*, 1053–1062.

Rowe, T., Aridor, M., McCaffery, J. M., Plutner, H., Nuoffer, C., and Balch, W. E. (1996). COPII vesicles derived from mammalian endoplasmic reticulum microsomes recruit COPI. J. Cell Biol. *135*, 895–911.

Rudolf, R., Magalhães, P. J., and Pozzan, T. (2006). Direct in vivo monitoring of sarcoplasmic reticulum Ca2+ and cytosolic cAMP dynamics in mouse skeletal muscle. J. Cell Biol. *173*, 187–193.

Rüegsegger, U., Leber, J. H., and Walter, P. (2001). Block of HAC1 mRNA translation by long-range base pairing is released by cytoplasmic splicing upon induction of the unfolded protein response. Cell *107*, 103–114.

Sacher, M., Barrowman, J., Wang, W., Horecka, J., Zhang, Y., Pypaert, M., and Ferro-Novick, S. (2001). TRAPP I implicated in the specificity of tethering in ER-to-Golgi transport. Mol. Cell *7*, 433–442.

Saraste, J., and Svensson, K. (1991). Distribution of the intermediate elements operating in ER to Golgi transport. J. Cell Sci. *100*, 415–430.

Scales, S. J., Pepperkok, R., and Kreis, T. E. (1997). Visualization of ER-to-Golgi transport in living cells reveals a sequential mode of action for COPII and COPI. Cell *90*, 1137–1148.

Shaywitz, D. A., Espenshade, P. J., Gimeno, R. E., and Kaiser, C. A. (1997). COPII subunit interactions in the assembly of the vesicle coat. J. Biol. Chem. *272*, 25413–25416.

Shibata, H., Suzuki, H., Yoshida, H., and Maki, M. (2007). ALG-2 directly binds Sec31A and localizes at endoplasmic reticulum exit sites in a Ca2+-dependent manner. Biochem. Biophys. Res. Commun. *353*, 756–763.

Trenker, M., Malli, R., Fertschai, I., Levak-Frank, S., and Graier, W. F. (2007). Uncoupling proteins 2 and 3 are fundamental for mitochondrial Ca2+ uniport. Nat. Cell Biol. *9*, 445–452.

Wahl, M., Sleight, R. G., and Gruenstein, E. (1992). Association of cytoplasmic free Ca2+ gradients with subcellular organelles. J. Cell Physiol. *150*, 593–609.

Williams, A. L., Ehm, S., Jacobson, N. C., Xu, D., and Hay, J. C. (2004). rsly1 binding to syntaxin 5 is required for endoplasmic reticulum-to-Golgi transport but does not promote SNARE motif accessibility. Mol. Biol. Cell *15*, 162–175.

Xu, D., and Hay, J. C. (2004). Reconstitution of COPII vesicle fusion to generate a pre-Golgi intermediate compartment. J. Cell Biol. *167*, 997–1003.

Xu, D., Joglekar, A. P., Williams, A. L., and Hay, J. C. (2000). Subunit structure of a mammalian ER/Golgi SNARE complex. J. Biol. Chem. *275*, 39631–39639.

Yamasaki, A., Tani, K., Yamamoto, A., Kitamura, N., and Komada, M. (2006). The Ca2+-binding protein ALG-2 is recruited to endoplasmic reticulum exit sites by Sec31A and stabilizes the localization of Sec31A. Mol. Biol. Cell *17*, 4876–4887.

Yu, S., Satoh, A., Pypaert, M., Mullen, K., Hay, J. C., and Ferro-Novick, S. (2006). mBet3p is required for homotypic COPII vesicle tethering in mammalian cells. J. Cell Biol. *174*, 359–368.

Zeuschner, D., Geerts, W. J., van Donselaar, E., Humbel, B. M., Slot, J. W., Koster, A. J., and Klumperman, J. (2006). Immuno-electron tomography of ER exit sites reveals the existence of free COPII-coated transport carriers. Nat. Cell Biol. *8*, 377–383.